J. Fluid Mech. (2009), *vol.* 628, *pp.* 241–268.
doi:10.1017/S0022112009006181 Printed in the United Kingdom

Analogy between velocity and scalar fields in a turbulent channel flow

ROBERT ANTHONY ANTONIA[1]†, HIROYUKI ABE[2] AND HIROSHI KAWAMURA[3]

[1]Discipline of Mechanical Engineering, University of Newcastle, NSW 2308, Australia
[2]Japan Aerospace Exploration Agency, Tokyo 182-8522, Japan
[3]Department of Mechanical Engineering, Tokyo University of Science, Chiba 278-8510, Japan

(Received 31 August 2008 and in revised form 18 January 2009)

The relationship between the fluctuating velocity vector and the temperature fluctuation has been examined using direct numerical simulation databases of a turbulent channel flow with passive scalar transport using a constant time-averaged heat flux at each wall for $h^+ = 180$, 395, 640 and 1020 (where h is the channel half-width with the superscript denoting normalization by wall variables) at Prandtl number $Pr = 0.71$. The analogy between spectra corresponding to the kinetic energy and scalar variance is reasonable in both inner and outer regions irrespective of whether the spectra are plotted in terms of k_x or k_z, the wavenumbers in the streamwise and spanwise directions respectively. Whereas all three velocity fluctuations contribute to the energy spectrum when k_x is used, the longitudinal velocity fluctuation is the major contributor when k_z is used. The quality of the analogy in the spectral domain is confirmed by visualizations in physical space and reflects differences between spatial organizations in the velocity and scalar fields. The similarity between the spectra corresponding to the enstrophy and scalar dissipation rate is not as good as that between the kinetic energy and scalar variance, emphasizing the prominence of the scalar sheets as the centre of the channel is approached. The ratio R between the characteristic time scales of the velocity and scalar fluctuations is approximately constant over a major part of the channel and independent of h^+, when the latter is sufficiently large. This constancy, which is not observed in quantities such as the turbulent Prandtl number, follows from the spectral similarities discussed in this paper and has implications for turbulent heat transport models.

1. Introduction

The transport of the instantaneous temperature in a turbulent flow is primarily controlled by the instantaneous velocity vector (e.g. Corrsin 1951; Batchelor 1959), with molecular effects tending to smooth out inhomogeneities in the smallest scales. While it is inappropriate to compare a scalar such as the temperature fluctuation θ which is lamellar in nature (e.g. Corrsin 1953) with a solenoidal vector such as the fluctuating velocity vector $\boldsymbol{q}$, it is reasonable to seek a similarity between the correlations $\overline{q(t)\cdot q(t+\tau)}$ and $\overline{\theta(t)\theta(t+\tau)}$, where the former quantity is the first invariant of the velocity correlation tensor $\overline{u_i(t)u_j(t+\tau)}$ (t and τ denote the time and a time delay, respectively; i or $j = 1$, 2, 3 represent the streamwise, wall-normal

† Email address for correspondence: robert.antonia@newcastle.edu.au

and spanwise directions, respectively; the overbar denotes the averaged value with respect to space and time). For the more common case, when $\tau = 0$, the transport equations for the mean turbulent kinetic energy $\overline{q^2}$ ($\equiv \overline{u^2} + \overline{v^2} + \overline{w^2}$) ($u$, v, w denote the streamwise, wall-normal and spanwise velocity fluctuations, respectively, and are sometimes used interchangeably with u_1, u_2, u_3) and mean temperature variance $\overline{\theta^2}$ are similar in form, when $Pr = 1$, except for the presence of the pressure diffusion term in the former equation (e.g. Fulachier & Antonia 1984). The similarity in the physical domain has a correspondence in the spectral domain. Indeed, there is experimental support for a spectral analogy between $\boldsymbol{q}$ and θ throughout most of the boundary layer (Fulachier & Dumas 1976) and in other turbulent shear flows (Fulachier & Antonia 1984). These imply that the same turbulence scales are major contributors to both $\overline{q^2}$and $\overline{\theta^2}$, a feature which may be exploitable in the context of developing reliable models for the transport of the scalar field. In the physical domain, an analogy has been established (Antonia *et al.* 1996) between the structure functions $(\delta u_i)^2$ and $(\delta\theta)^2$; the transport equations for these two quantities provide some support for this analogy at least within the framework of homogeneity and isotropy (Antonia *et al.* 1997) when the molecular Prandtl number, Pr, is 1. It should also be noted that this spectral analogy breaks down (see chapter 7 of Chassaing *et al.* 2002) when the source (production) terms for $\overline{q^2}$ and $\overline{\theta^2}$ are not maintained, as is the case in grid turbulence. In flows in which there is a constant source of velocity and scalar fluctuations due to the presence of a wall, such as in a boundary layer or a channel flow, the spectral analogy appears to be reasonably well supported by the available experimental and numerical data, especially as the wall is approached. It is also supported in the absence of a wall but in the presence of both mean velocity and temperature gradients, for example in the case of a uniform shear flow with a constant mean temperature gradient (e.g. Tavoularis & Corrsin 1981). The previous comments imply that for the analogy to be valid, some forcing must be applied, although it is not yet clear if the scalar needs to be forced separately from the velocity field, given that the scalar should feel the influence of the fluctuating strain rate even for values of Pr close to unity. In this context, with a single or multiple (for example via a heated mandoline) localized heat sources at the entrance of a channel, one would expect the analogy to be satisfied in the fully developed region of the channel once the temperature has been sufficiently mixed by the large-scale motion. In the absence of external forcing, as in decaying turbulence downstream of a grid or along the axes of jet and wake flows, the analogy is not tenable. The experimental evidence gathered by Burattini & Antonia (2005) indicates that in decaying-type flows, the second-order temperature structure function $(\delta\theta)^2$ behaves as if it were 'forced', a behaviour consistent with that noted by Warhaft (2000).

Direct numerical simulations (DNSs) provide more reliable information than measurements, especially in the near-wall region (e.g. Moin & Mahesh 1998). The DNS database of Kim & Moin (1989) was exploited by Antonia & Kim (1991) who examined the spectral analogy between $\boldsymbol{q}$ and θ in the near-wall region of a turbulent channel flow at a low Reynolds number ($h^+ = u_\tau/\nu = 180$, where u_τ is the friction velocity, ν the kinematic viscosity and h the channel half-width; the superscript denotes normalization by wall variables), with three values of the molecular Prandtl number ($Pr = 0.1$, 0.71 and 2). The analogy, presented only in terms of k_x, was quite satisfactory for $Pr = 0.71$, but the dependence on Pr of the temperature spectrum becomes more pronounced with increasing distance from the wall, thus implying an impairment of the analogy as the distance from the wall is increased. Commonly, measured spectra are presented only in terms of k_x,

after Taylor's hypothesis is invoked for converting the frequency to a streamwise wavenumber. The use of DNS data circumvents the need for Taylor's hypothesis and allows spectra to be examined in terms of both k_x and k_z, which respectively are the wavenumbers in the streamwise and spanwise directions. While measurements can provide useful information about the spatial organization of velocity and scalar fields (indeed, evidence for the close similarity between velocity and thermal streaks was first obtained experimentally by Iritani, Kasagi & Hirata 1985, while evidence for the 'cliff-ramp' like spatial structure of temperature was first evidenced in the atmospheric surface layer measurements by Taylor 1958), DNS databases allow detailed simultaneous three-dimensional examinations of the instantaneous velocity and scalar fields.

In the present study, we examine the analogy via both streamwise and spanwise spectra with the use of the DNS databases for a fully developed channel flow with a passive scalar for four values of the Reynolds number ($h^+ = 180$, 395, 640 and 1020) at $Pr = 0.71$ (Abe, Kawamura & Matsuo 2004*b*; Abe, Antonia & Kawamura 2008, 2009). There are two major objectives. The first is to clarify and quantify the extent of the similarity between the $\boldsymbol{q}$ and θ spectra throughout the channel, both in physical space and in the spectral domain, for several values of h^+. We present spectra (in § 3) both with respect to k_x and k_z in order to assess the relative contributions from the three velocity fluctuations to the turbulent kinetic energy and with those from the temperature fluctuations to the temperature variance in each case. Note that spectra with respect to k_y (the wavenumber in the wall-normal direction) are not obtainable in the present flow due to the inhomogeneity in the y direction. Since the quality of the analogy is likely to be linked to the degree of similarity between the spatial organizations of the velocity and scalar fields, instantaneous q^2 and θ^2 contours are viewed in the (x, y), (x, z) and (y, z) planes (x, y, z represent the streamwise, wall-normal and spanwise directions, respectively.). The second objective is to explore the possibility of a spectral analogy between the scales responsible for the dissipation rates of $\overline{q^2}$ and $\overline{\theta^2}$, thus extending the scope of the earlier work (Fulachier & Dumas 1976; Fulachier & Antonia 1984; Antonia & Kim 1991). One expects that turbulence scales that are responsible for dissipating turbulent kinetic energy as heat would also play a dominant role in scrambling or destroying the temperature fluctuations. An analogy between the enstrophy and temperature dissipation rate spectra is suggested by the similarity between the transport equations for the mean enstrophy and mean scalar dissipation rate (Corrsin 1953; Abe *et al.* 2008, 2009). Intuitively, the close similarity between the velocity and thermal streaks near the wall should lead to a close relationship between at least some of the vorticity and scalar derivative components due to the concentrations of the velocity and scalar derivatives in the regions between low-speed and high-speed streaks (or alternately between low-temperature and high-temperature streaks) and hence a high degree of correlation between the enstrophy (or energy dissipation rate) and the scalar dissipation rate in the wall region. This should in turn be reflected in a similarity between the corresponding spectra. It is evident that in order to test this similarity, high-quality small-scale data are required. This requirement is quite difficult, if not insurmountable, experimentally but achievable with adequately resolved DNS databases. Accordingly, the likely analogy between spectra associated with the energy and scalar dissipation rate scales is assessed in § 4. In § 5, an attempt is made to quantify the quality of the spectral similarity between $\boldsymbol{q}$ and θ and also that between the enstrophy (or energy dissipation rate) and the scalar dissipation rate. This section also considers the implication of these two types of similarity on the dissipation time-scale ratio.

2. DNS details

The present databases have been obtained from DNSs in a turbulent channel flow with passive scalar transport by Abe *et al.* (2004*b*, 2008, 2009). Four values of h^+ (180, 395, 640 and 1020) are used. The molecular Prandtl number is 0.71. The flow is a fully developed turbulent channel flow driven by a constant streamwise mean pressure gradient. For the scalar (temperature) field, the conservation (energy) equation has been time-integrated. The thermal boundary condition is the same as that used by Kasagi, Tomita & Kuroda (1992). A constant time-averaged heat flux is applied at each wall. This implies that the wall temperature, averaged over the z direction and time, increases linearly in the x direction. Similarly, the bulk mean temperature also increases linearly in the x direction. The wall temperature fluctuation is assumed to be zero. In this context, the introduction of the temperature difference Θ defined as

$$T = \frac{\partial \langle T_w \rangle}{\partial x} x - \Theta \tag{2.1}$$

(T and T_w are the local temperature and wall temperature, respectively; the angular bracket represents integration over z and t) enables the use of the no-slip boundary condition in the y direction. For the other (x and z) directions, periodic boundary conditions are imposed. The governing equation for the scalar field can then be written as

$$\frac{\partial \Theta^+}{\partial t^\#} + U_j^+ \frac{\partial \Theta^+}{\partial x_j^\#} = \frac{1}{h^+ \cdot \mathrm{Pr}} \frac{\partial^2 \Theta^+}{\partial x_j^{\#2}} + U_1^+ \frac{2}{\int_0^2 \bar{U}_1 \mathrm{d}y^\#} \tag{2.2}$$

(see also Kasagi *et al.* 1992; Kasagi & Ohtsubo 1993; Kawamura *et al.* 1998), where the superscript # denotes normalization by the channel half-width (h), and the capital letters represent instantaneous values. In view of the last term of (2.2), the time-averaged heat flux remains constant across the channel. Note that the present thermal boundary condition differs from the conditions used by Kim & Moin (1989). For the first of these, an internal heat source was used so that the passive scalar was created internally and removed at both walls. In the second, the source was turned off and the scalar was introduced at the lower wall and removed at the upper wall.

A fractional step method is used with semi-implicit time advancement. The third-order Runge–Kutta method (Spalart, Moser & Rogers 1991) is used for the viscous terms in the y direction and the Crank–Nicolson method is used for the other terms. A finite-difference method is adopted for the spatial discretization. A fourth-order central scheme (Morinishi *et al.* 1998) is used in the x and z directions, while a second-order central scheme is used in the y direction. For the initial velocity condition, an instantaneous velocity field corresponding to a fully developed state was taken from an earlier DNS of a turbulent channel flow. For the initial temperature condition, the mean temperature distribution, as given by Kader's (1981) formula, was assumed (as in Kasagi & Ohtsubo 1993). The time integration was typically carried out to several thousand times the viscous time scale (ν/u_τ^2) until the scalar field was deemed, primarily on the basis of the total heat-flux distribution, to have reached a fully developed state. Further details on the simulations are given in Abe, Kawamura & Matsuo (2001) and Abe *et al.* (2004*b*, 2008, 2009), and the reader may refer to these papers as well as Kawamura, Abe & Matsuo (2004) for information on basic turbulence statistics such as mean and root mean square (r.m.s.) temperatures and turbulent heat fluxes.

The computational domain size ($L_x \times L_y \times L_z$), number of grid points ($N_x \times N_y \times N_z$) and spatial resolution (Δx, Δy, Δz) are given in table 1 in which the superscript *

h^+	180	395	640	1020
$L_x \times L_y \times L_z$		$12.8h \times 2h \times 6.4h$		
$L_x^+ \times L_y^+ \times L_z^+$	$2304 \times 360 \times 1152$	$5056 \times 790 \times 2528$	$8192 \times 1280 \times 4096$	$13\,056 \times 2040 \times 6528$
$N_x \times N_y \times N_z$	$768 \times 128 \times 384$	$1536 \times 192 \times 768$	$2048 \times 256 \times 1024$	$2048 \times 448 \times 1536$
Δx^+, Δy^+, Δz^+	3.00, 0.20 ~ 5.90, 3.00	3.29, 0.15 ~ 6.52, 3.29	4.00, 0.15 ~ 8.02, 4.00	6.38, 0.15 ~ 7.32, 4.25
Δx_w^*, Δy_w^*, Δz_w^*	1.94, 0.13, 1.94	2.24, 0.10, 2.24	2.77, 0.11, 2.77	4.46, 0.11, 2.97
Δx_c^*, Δy_c^*, Δz_c^*	0.82, 1.62, 0.82	0.74, 1.47, 0.74	0.82, 1.64, 0.82	1.16, 1.33, 0.77

TABLE 1. Domain size, grid points and spatial resolution of the DNS databases.

denotes normalization by Kolmogorov scales, and the subscripts w and c refer to the wall and centreline, respectively. Since the spatial resolution at $h^+ = 180$, 395 and 640 is finer than for $h^+ = 1020$, a detailed study of the small scales was made (Abe *et al.* 2008, 2009) at only the three smaller Reynolds numbers. In the present context, it seemed appropriate to examine the spectral analogy between the turbulent kinetic energy and the scalar variance at all four values of h^+. However, only the three smaller values of h^+ were used when comparing spectra corresponding to the dissipation rates of the turbulent energy and scalar variance. The present spatial resolution is comparable with that of del Álamo *et al.* (2004) and Hoyas & Jiménez (2008) in the y direction but is somewhat finer in the x and z directions. In particular, the spatial resolution is good at the centreline, since Δx^* and Δz^* are smaller than 1 and Δy^* is smaller than about 1.6. At the wall, the poorest resolution is in the x direction (table 1), but this is unlikely to have a major effect on streamwise spectra, since the magnitudes of the velocity and scalar streamwise derivatives are quite small near the wall (see Antonia, Kim & Browne 1991; Abe, Antonia & Kawamura 2006; Abe *et al.* 2009). As will be evident in the following sections, there is no spurious behaviour in the spectra at or near the most energetic scales. While L_x and L_z are about half as large as for del Álamo *et al.* (2004) and Hoyas & Jiménez (2008), the energy-containing scales are much smaller than L_x and L_z so that the effect of the domain size on basic turbulence statistics is negligibly small (see Abe, Kawamura & Choi 2004*a*). The previous considerations suggest that, overall, the spatial resolution and domain size should be adequate for the present purpose, viz. for analysing the analogy between spectra corresponding to the mean turbulent kinetic energy and mean scalar variance as well as that between spectra corresponding to the dissipation rates of these two quantities.

3. Analogy between the turbulent kinetic energy and scalar variance

One-dimensional streamwise and spanwise spectral densities are defined such that

$$\int_0^\infty F_\beta(k_x)\,\mathrm{d}k_x = \int_0^\infty F_\beta(k_z)\,\mathrm{d}k_z = 1\,, \tag{3.1}$$

where β stands for either u, v, w (streamwise, wall-normal and spanwise velocity fluctuations, respectively) or θ (temperature fluctuation). With the use of F_u, F_v, F_w, the spectrum of $\boldsymbol{q}$ is obtained as

$$F_q = (\overline{uu}/\overline{qq})\ F_u + (\overline{vv}/\overline{qq})\ F_v + (\overline{ww}/\overline{qq})\ F_w \tag{3.2}$$

Figure 1 shows the streamwise and spanwise spectral densities of $\boldsymbol{q}$ and θ for $h^+ = 180$, 395, 640 and 1020 at $Pr = 0.71$ in the inner region, where F_u is included for

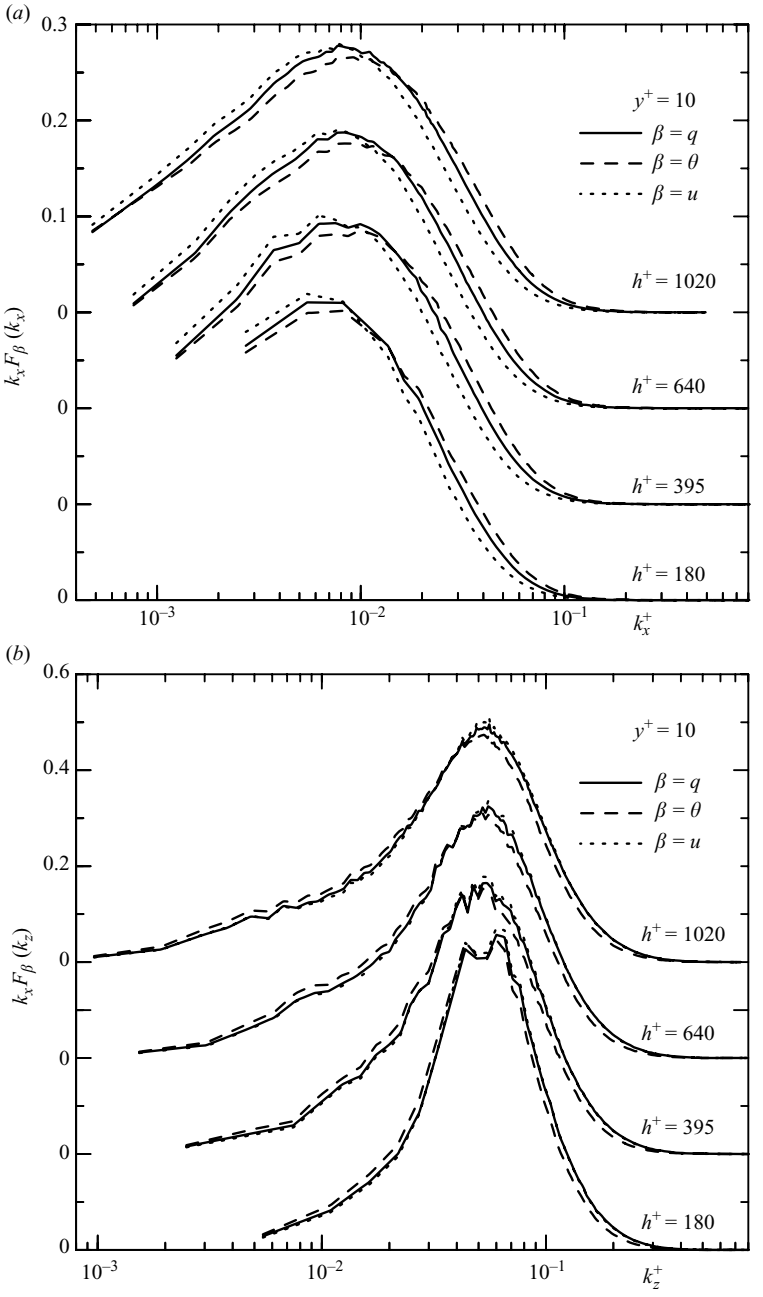

FIGURE 1. One-dimensional pre-multiplied spectral density of q, θ and u for $h^+ = 180$, 395, 640 and 1020 at $y^+ = 10$: (*a*) streamwise spectra; (*b*) spanwise spectra. Note the shift in origin for the ordinate. The lowest zero refers to $h^+ = 180$.

comparison. Note that both streamwise and spanwise spectral densities are multiplied by the corresponding wavenumber and are plotted using log–linear (abscissa–ordinate) scales so as to readily allow the identification of the scales which contribute most to the turbulent energy or scalar variance. As for the turbulent boundary layer

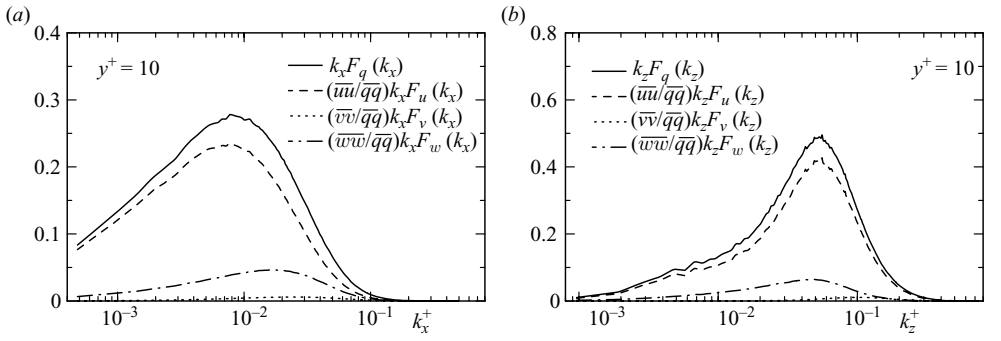

FIGURE 2. One-dimensional pre-multiplied spectral density of u, v, w and q for $h^+ = 1020$ at $y^+ = 10$: (a) streamwise spectra; (b) spanwise spectra.

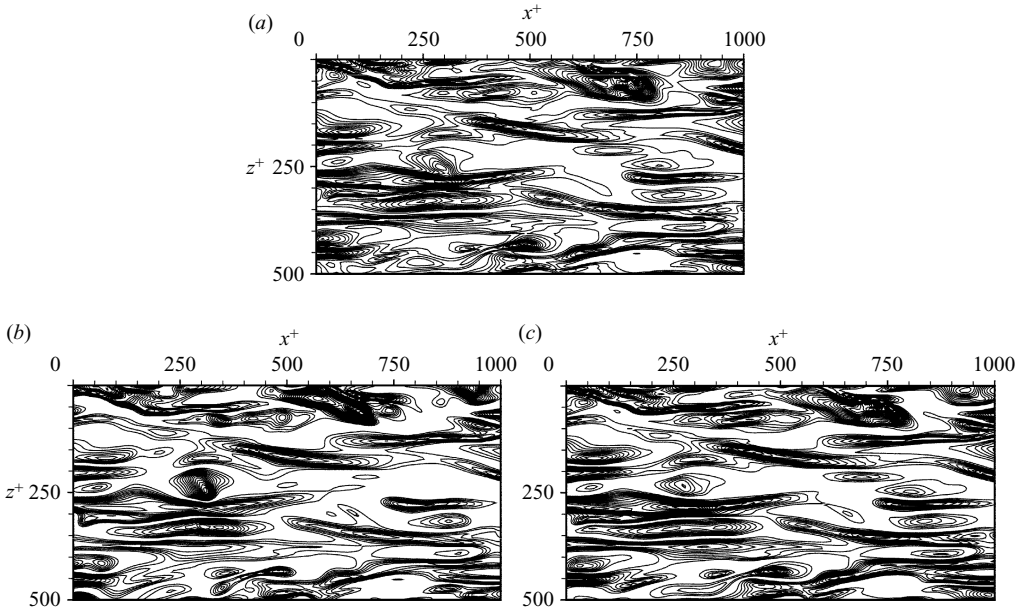

FIGURE 3. Instantaneous (x, z) isocontours of q^2, θ^2 and u^2 for $h^+ = 1020$ at $y^+ = 10$: (a) $q^2/\overline{q^2}$; (b) $\theta^2/\overline{\theta^2}$; ($c$) $u^2/\overline{u^2}$.

experiment of Fulachier & Dumas (1976), the present results indicate that F_q and F_θ follow each other closely for nearly the whole wavenumber range, almost independent of h^+. In the near-wall region, this similarity is marginally better than that between F_u and F_θ (see F_θ / F_u and F_θ / F_q at $y^+ = 10$ in figure 16), even though the largest contribution to F_q near the wall is from the streamwise velocity fluctuation (figure 1). This implies that in the context of the spectral similarity, the contribution of F_w to F_q cannot be dismissed (see figure 2), consistent with the low h^+ results of Antonia & Kim (1991).

The near-wall correspondence observed in the spectra is reflected in physical space. Figure 3 shows isocontours of q^2 and θ^2 together with those of u^2 (each instantaneous field has been normalized by its own mean square value obtained from the instantaneous (x, z) plane data) for $h^+ = 1020$ at $y^+ = 10$. Note that in figure 3,

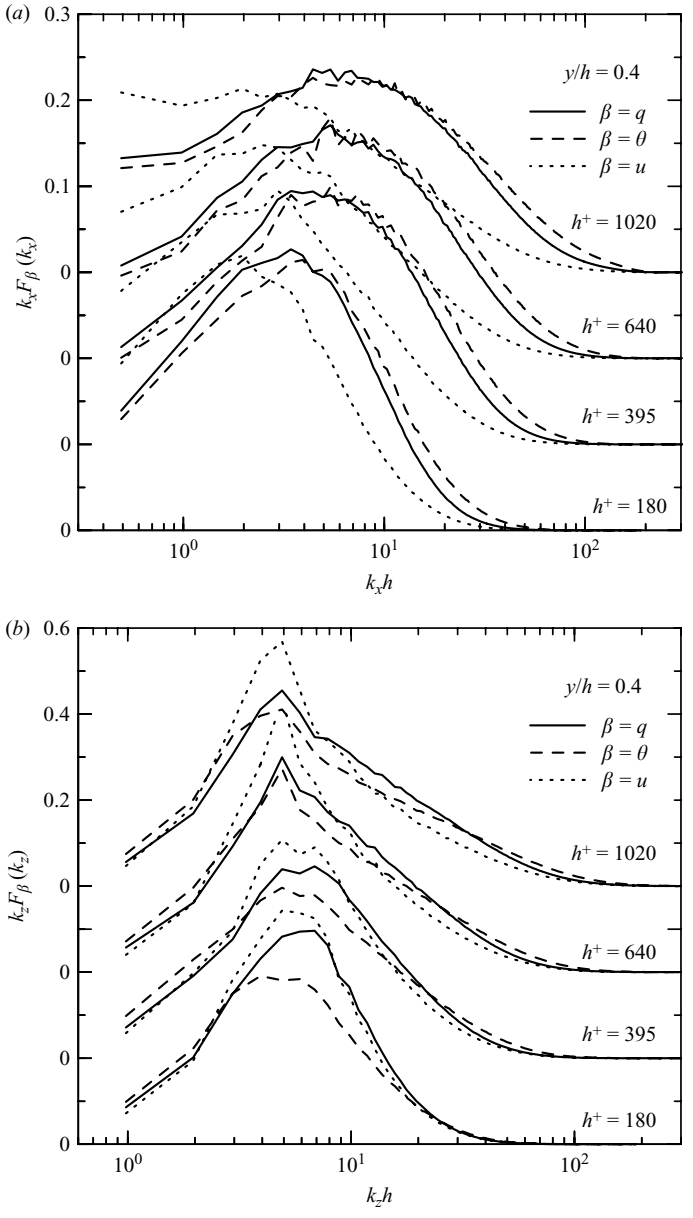

FIGURE 4. One-dimensional pre-multiplied spectral density of q, θ and u for $h^+ = 180$, 395, 640 and 1020 at $y/h = 0.4$: (*a*) streamwise spectra; (*b*) spanwise spectra. Note the shift in origin for the ordinate. The lowest zero refers to $h^+ = 180$.

line contours are used instead of shaded contours to emphasize the large magnitudes. The correspondence between q^2 and θ^2 is slightly better than that between u^2 and θ^2, although the similarity between u^2 and θ^2 is high in the near-wall region (e.g. Iritani, Kasagi & Hirata 1985; Antonia, Krishnamoorthy & Fulachier 1988; Kim & Moin 1989; Kasagi *et al.* 1992; Kasagi & Ohtsubo 1993).

In the outer region, as in the inner region, the spectral analogy between $\boldsymbol{q}$ and θ generally holds for all wavenumbers (figure 4) with the exception of the spanwise

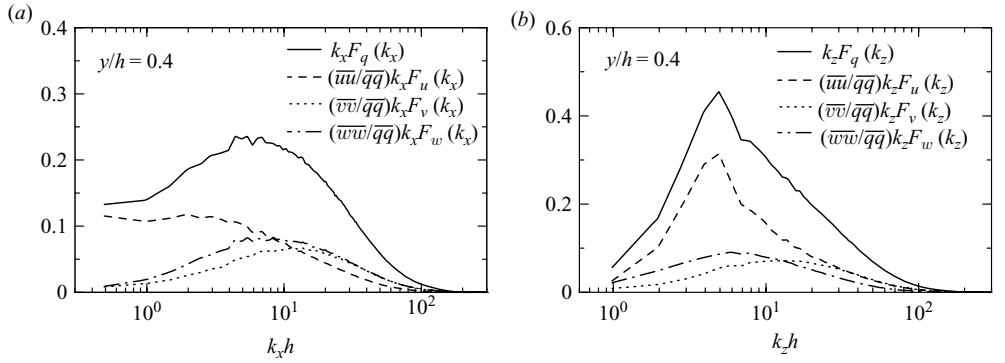

FIGURE 5. One-dimensional pre-multiplied spectral density of u, v, w and q for $h^+ = 1020$ at $y/h = 0.4$: (*a*) streamwise spectra; (*b*) spanwise spectra.

spectra at low h^+(180 and 395), which may be due to an insufficient separation between large and small scales. However, the reason for the similarity between F_q and F_θ cannot be explained simply, since the relative contributions of F_u, F_v, F_w to F_q are different in the x and z directions (figure 5). For the streamwise spectra, all three velocity fluctuations contribute almost equally to $\boldsymbol{q}$ at the most energetic scales so that the spectral peaks in F_q reside at higher wavenumbers than those for F_u (figure 5*a*), while for the spanwise spectra, u contributes mostly to $\boldsymbol{q}$ so that the spectral peaks in F_q are almost the same as those in F_u (figure 5*b*). Hence, the spanwise spectral similarity between $\boldsymbol{q}$ and θ is mainly attributed to that between u and θ, while the streamwise similarity between $\boldsymbol{q}$ and θ reflects the sum of similarities between u and θ, v and θ and w and θ. Inspection of the streamwise co-spectra of v and θ in the outer region indicated that the most energetic wavenumbers are close to those of the v and θ spectra (not shown here), implying a close relationship between v and θ in this region.

A few previous studies focused on the most energetic peak wavenumbers (or wavelengths) of the spectra in the outer region of this flow (e.g. Jiménez 1998; del Álamo & Jiménez 2003; Abe *et al.* 2004*a*). For the spanwise spectra, del Álamo & Jiménez (2003) reported the spanwise most energetic peak wavelength of the u spectrum to be about $2h$ in the outer region. Abe *et al.* (2004*a*) suggested that the peak wavelength is about $1.3h$, independent of h^+, and is associated with the spanwise spacing of large-scale u structures. There is also evidence for the similarity between the spanwise spacing of large-scale u and θ structures in this region as reported by Kawamura *et al.* (2004). For the streamwise spectra, on the other hand, del Álamo & Jiménez (2003) reported the streamwise most energetic peak wavelength of the u spectrum to be $2h$–$5h$ in the outer region. Recently, Hutchins & Marusic (2007) analysed the DNS database of del Álamo *et al.* (2004) and indicated the existence of very long u structures, more than $25h$ in length, in the logarithmic region. They also presented evidence on the very large-scale structures, using the DNS database obtained with the largest computational domain ($8\pi h$ in the x direction) used to date. The present study has revealed that the most energetic wavelengths of θ and $\boldsymbol{q}$ are much shorter than those of u and are of the order of h in the outer region (figure 4), suggesting that the turbulent kinetic energy and scalar variance are substantially composed of scales much smaller than those associated with the very large-scale structures. This finding may suggest one reason why turbulence statistics

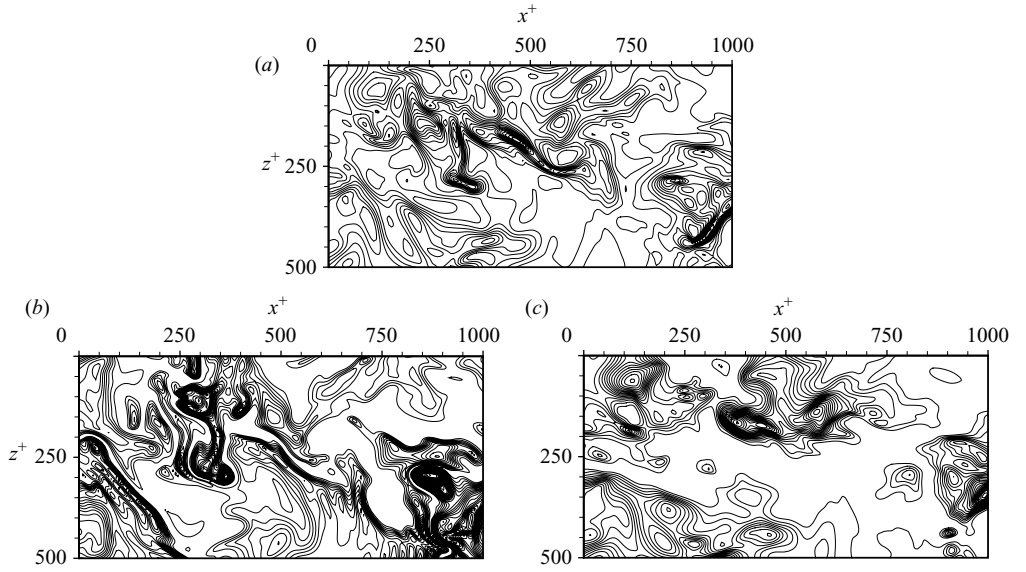

FIGURE 6. Instantaneous (x, z) isocontours of q^2, θ^2 and u^2 for $h^+ = 1020$ at $y/h = 0.4$: (a) $q^2/\overline{q^2}$; (b) $\theta^2/\overline{\theta^2}$; (c) $u^2/\overline{u^2}$.

can be obtained adequately, if not accurately, without completely resolving the very large-scale structures in recent DNSs of this flow.

The similarity between q^2 and θ^2 isocontours (figure 6) is not as good in the outer region; the correlation coefficient (0.35) for figure 6 is less than half that (0.76) for figure 3 (the correlation coefficient is defined such that $\rho_{\phi\varphi} \equiv \overline{(\phi - \bar{\phi})(\varphi - \bar{\varphi})}/\sigma_\phi \sigma_\varphi$, where sigma denotes the r.m.s. value; here, the mean and r.m.s. values are calculated from the instantaneous (x, z) plane data). However, while $\rho_{q^2\theta^2}$ as well as $\rho_{u^2\theta^2}$ and $\rho_{w^2\theta^2}$ are larger in the inner region ($\rho_{u^2\theta^2} = 0.77$, $\rho_{w^2\theta^2} = 0.10$) than in the outer region ($\rho_{u^2\theta^2} = 0.34$, $\rho_{w^2\theta^2} = 0.04$), $\rho_{v^2\theta^2}$ in the outer region (0.19) is larger than that in the inner region (0.11). The increased correlation between θ^2 and v^2 can be readily confirmed in instantaneous views when the focus is only on large magnitudes. Although contours of θ^2 and v^2 are not shown here, we refer to the location $x^+ = z^+ = 250$ in figure 6 which emphasizes that the similarity between large magnitudes of q^2 and θ^2 is superior to that between u^2 and θ^2, even though $\rho_{q^2\theta^2}$ (0.35) and $\rho_{u^2\theta^2}$ (0.34) are approximately equal. Consequently, the spectral similarity reported here is consistent with the information contained in the instantaneous contours, provided the eye focuses only on the most energetic scales when viewing these contours. The present observations in physical space suggest that θ is affected by v and w as well as u in the outer region. The spanwise extent of the large-scale θ structures is thus bigger than that of the large-scale u structures (figure 6), which is one notable difference between large-scale u and θ structures in the outer region.

The similarity between large magnitudes of q^2 and θ^2 in the instantaneous (x, z) plane views is also observed in instantaneous (x, y) and (y, z) plane views. One example is given in figure 7, where isocontours of q^2 and θ^2 in the (x, y) plane for $h^+ = 1020$ are shown together with those of u^2. Figure 7 displays another difference between the u and θ large-scale structures in the outer region. The inclination of the large-scale θ structures to the wall is greater than that of the large-scale u structures (see also the coloured isocontours of u and θ in figure 8), consistent with

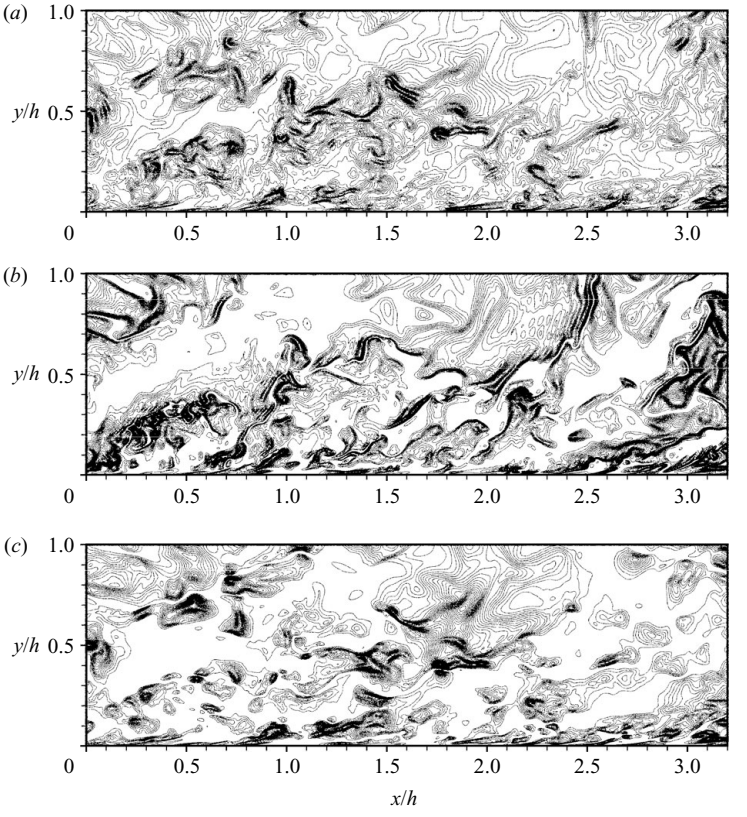

FIGURE 7. Instantaneous (x, y) isocontours of q^2, θ^2 and u^2 for $h^+ = 1020$: (*a*) $q^2/\overline{q^2}$; (*b*) $\theta^2/\overline{\theta^2}$; (*c*) $u^2/\overline{u^2}$.

the differences between the two-point correlations in the (x, y) plane for u and θ as reported by Kawamura *et al.* (2002) (see also figure 9). In this context, the average inclination of the large-scale u structures to the wall lies in the range 12°–30° for turbulent boundary layer and channel flows (e.g. Brown & Thomas 1977; Rajagopalan & Antonia 1979; Robinson 1991; Krogstad & Antonia 1994; Christensen & Adrian 2001), whereas the inclination of the large-scale θ structures to the wall is in the range 26°–52° for the laboratory and atmospheric surface layers (see Antonia *et al.* 1979 and the references therein). The inclination angles shown in figures 7–9 are consistent with those in the references cited above.

There is a difference (figure 8) associated with the interfaces between positive and negative values of large-scale θ and u structures (fronts or backs). Even though the Prandtl number is moderate (0.71), the interfaces of θ are sharper than those of u, which seems to be in conformity with the greater amount of energy observed in θ than in u at high wavenumbers (figure 4). This behaviour is also consistent with measurements in thermal boundary layers (Chen & Blackwelder 1978; Antonia *et al.* 1982; Subramanian *et al.* 1982). Further, at the interfaces, θ is more likely to be less mixed than u, especially in the outer region. This may be associated with the unmixedness of the scalar, as suggested by Guezennec, Stretch & Kim (1990) for a turbulent channel flow with one wall heated and the other cooled, who suggested that there may exist significant differences between the local transports of heat and

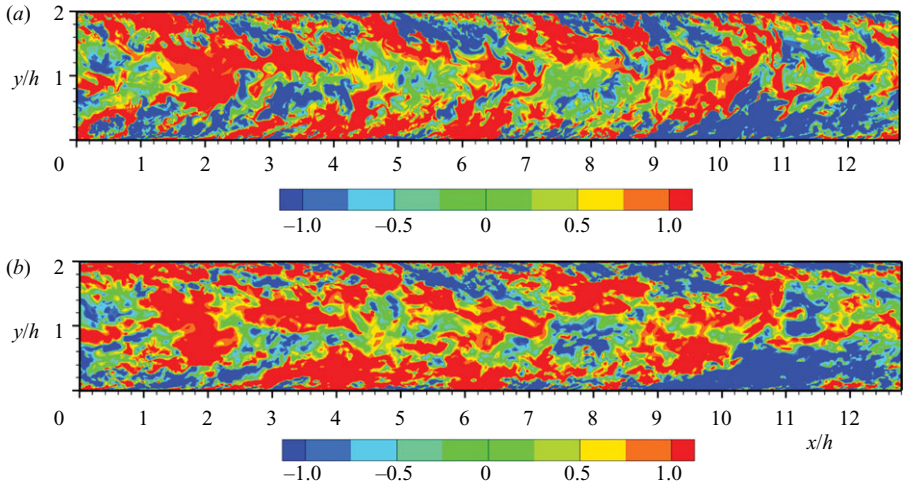

FIGURE 8. Instantaneous (x, y) colour isocontours of θ and u for $h^+ = 1020$: (a) θ^+; (b) u^+.

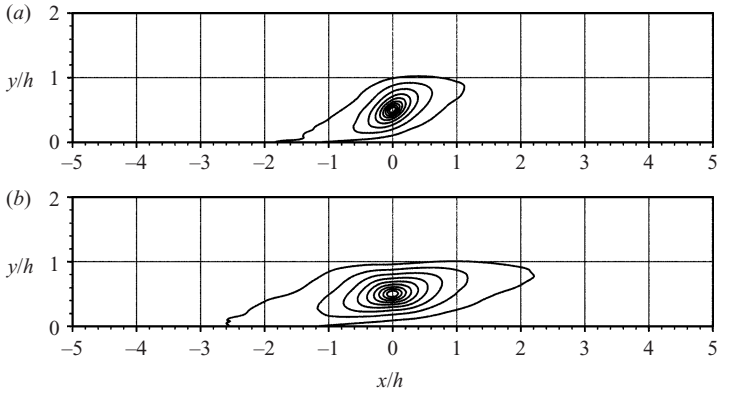

FIGURE 9. Two-dimensional (x, y) two-point correlations of u and θ at $h^+ = 395$ for the reference y location of $y/h \approx 0.5$: (a) θ; (b) u. Contour levels are from 0.1 to 0.9 with the increment of 0.1.

momentum due to the role played by the pressure fluctuations, even when Pr is of the order of unity, and pointed out that the temperature, which seems to appear in concentrated form around the eddies, retains a higher degree of unmixedness than the velocity.

How does the similarity between $\boldsymbol{q}$ and θ vary with respect to y? Spectra (not shown here) at several y locations in the wall region confirm that the similarity between the $\boldsymbol{q}$ and θ spectra is quite good for either streamwise or spanwise wavenumbers. With increasing distance from the wall, the similarity between the $\boldsymbol{q}$ and θ spectra is not as good, implying that the large near-wall magnitudes of the mean velocity and temperature gradients are important in the context of the closeness of the similarity in that region. Nonetheless, in both the logarithmic and outer regions, the similarity between the $\boldsymbol{q}$ and θ spectra is superior to that between the u and θ spectra. The peak of the u spectrum is located at lower wavenumbers than that of the streamwise

$\boldsymbol{q}$ and θ spectra, while the peak of the spanwise u spectrum is much sharper than that of the spanwise $\boldsymbol{q}$ or θ spectra. These results suggest that, overall, the similarity between the $\boldsymbol{q}$ and θ spectra is satisfactory throughout the channel, consistent with the turbulent boundary layer results of Fulachier & Dumas (1976). The analogy may be useful for developing more reliable turbulence models for the scalar field, such as the k_θ–χ (scalar variance–scalar dissipation rate) model (e.g. Nagano & Kim 1988; Yoshizawa 1988, Nagano & Shimada 1996). The present finding is also important from an experimental context, since the $\boldsymbol{q}$ spectra can be inferred from the θ spectra without the need to measure the three velocity components.

4. Analogy between scales associated with the dissipation rates of the turbulent kinetic energy and scalar variance

We next explore the possibility of a spectral analogy between scales associated with the dissipation rates of $\overline{q^2}$ and $\overline{\theta^2}$. For small-scale turbulence, an analogy between the transport equations for the mean enstrophy $\overline{\omega_i^2}$ and $\overline{\theta,_i^2}$, which is sometimes referred to as the mean scalar enstrophy, was first established by Corrsin (1953). Note that $\overline{\theta,_i^2}$ and the mean scalar dissipation rate $\overline{\chi} = \kappa(\overline{\theta,_i^2})$ differ only through the factor κ (thermal diffusivity). Recently, Abe *et al.* (2008, 2009) have presented support for this analogy using DNS databases for the present flow. In this section, the analogy between the enstrophy spectrum F_ω and the scalar dissipation spectrum F_χ defined as

$$F_\omega = (\overline{\omega_1\omega_1}/\overline{\omega_i\omega_i})\, F_{\omega_1} + (\overline{\omega_2\omega_2}/\overline{\omega_i\omega_i})\, F_{\omega_2} + (\overline{\omega_3\omega_3}/\overline{\omega_i\omega_i})\, F_{\omega_3}, \tag{4.1}$$

$$F_\chi = (\overline{\theta,_1\,\theta,_1}/\overline{\theta,_i\,\theta,_i})\, F_{\theta,_1} + (\overline{\theta,_2\,\theta,_2}/\overline{\theta,_i\,\theta,_i})\, F_{\theta,_2} + (\overline{\theta,_3\,\theta,_3}/\overline{\theta,_i\,\theta,_i})\, F_{\theta,_3} \tag{4.2}$$

(ω_i and $\theta,_i \equiv \partial\theta/\partial x_i$ denote the fluctuating vorticity and scalar derivative components in the ith direction, respectively) is examined in both inner and outer regions. The choice of ω_i^2 instead of ε ($\equiv \nu(u_{i,j}(u_{i,j} + u_{j,i}))$) as the representative small-scale quantity may be justified by the fact that for homogeneous turbulence the relationship between the mean turbulent energy dissipation rate $\overline{\varepsilon}$ and the mean enstrophy, $\overline{\omega_i^2}$, is given by

$$\overline{\varepsilon} = \nu\,\overline{\omega_i\omega_i}. \tag{4.3}$$

Antonia *et al.* (1991) found that for $h^+ = 180$ and 395, this equality is satisfied approximately throughout the channel. The present data confirm this at all values of h^+. The largest departure (less than 5 %) from 1 of the ratio of $\nu\,\overline{\omega_i\omega_i}$ and the exact dissipation rate (ε) occurs in the wall region ($y^+ = 5$) (see also Abe *et al.* 2009). Since the spectra (not shown here) corresponding to ω_i^2 are almost indistinguishable from those which correspond to ε at all locations in the channel, the results in this section should apply equally well for F_ε as they do for F_ω. Note that the use of (4.3) allows $\overline{\varepsilon}$ to be readily determined experimentally from a three-component vorticity probe (e.g. Antonia, Zhou & Zhu 1998).

Figure 10 displays the streamwise and spanwise spectral densities of ω_i^2 and χ for $h^+ = 180$, 395 and 640 at $Pr = 0.71$ in the inner region. The correspondence between F_ω and F_χ is good for both streamwise and spanwise spectra, although the quality of the collapse for F_q and F_θ is slightly better than that for F_ω and F_χ (see figures 1 and 10). The similarity between F_ω and F_χ mainly reflects that between F_{ω_3} and $F_{\theta,_2}$ and between F_{ω_2} and $F_{\theta,_3}$ (figure 11), consistent with the high degrees of similarity between ω_2 ($\simeq u,_3$) and $\theta,_3$ (viz. spanwise interfaces of momentum and thermal streaks) and between ω_3 ($\simeq -u,_2$) and $\theta,_2$ (viz. edges of momentum and thermal streaks) in the

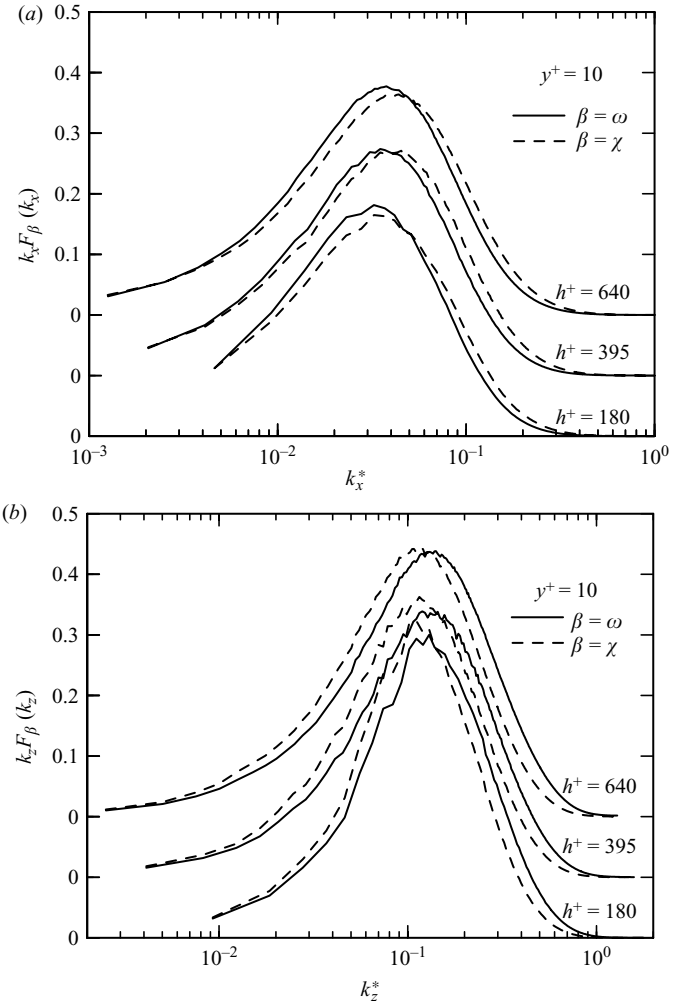

FIGURE 10. One-dimensional pre-multiplied spectral density of ω and χ for $h^+ = 180$, 395 and 640 at $y^+ = 10$: (*a*) streamwise spectra; (*b*) spanwise spectra. Note the shift in origin for the ordinate. The lowest zero refers to $h^+ = 180$.

near-wall region (Abe *et al.* 2006, 2009). Hence, the dissimilarity between F_ω and F_χ in this region is attributed to that between F_{ω_1} and $F_{\theta,1}$. Careful inspection of figure 11 has shown that the magnitude of F_{ω_1} is much larger than that of $F_{\theta,1}$ for all wavenumbers, the magnitude of $F_{\theta,1}$ being negligibly small. One may notice another difference in the most energetic peak wavenumbers for F_{ω_i} (figure 11*a*, *c*), reflecting the different spatial size or spacing of ω_i near the wall (e.g. Robinson 1991). These differences lead to a similarity between F_ω and F_χ of smaller quality than that between F_q and F_θ. The visualizations in physical domain support the analogy between F_ω and F_χ. Figure 12 shows isocontours of ω_i^2 and χ together with those of ε (each instantaneous field has been normalized by its own mean value) for $h^+ = 640$ at $y^+ = 10$. Again, the similarity between ω_i^2 and χ is satisfactory but is inferior to that between q^2 and θ^2 (see figures 3 and 12). Note that the similarity between ε and χ is nearly identical with that between ω_i^2 and χ, since $\omega_i^2 \approx \varepsilon$ near the wall (the correlation coefficients $\rho_{\varepsilon\chi}$ and $\rho_{\omega_i^2\chi}$ are approximately equal; Abe *et al.* 2009).

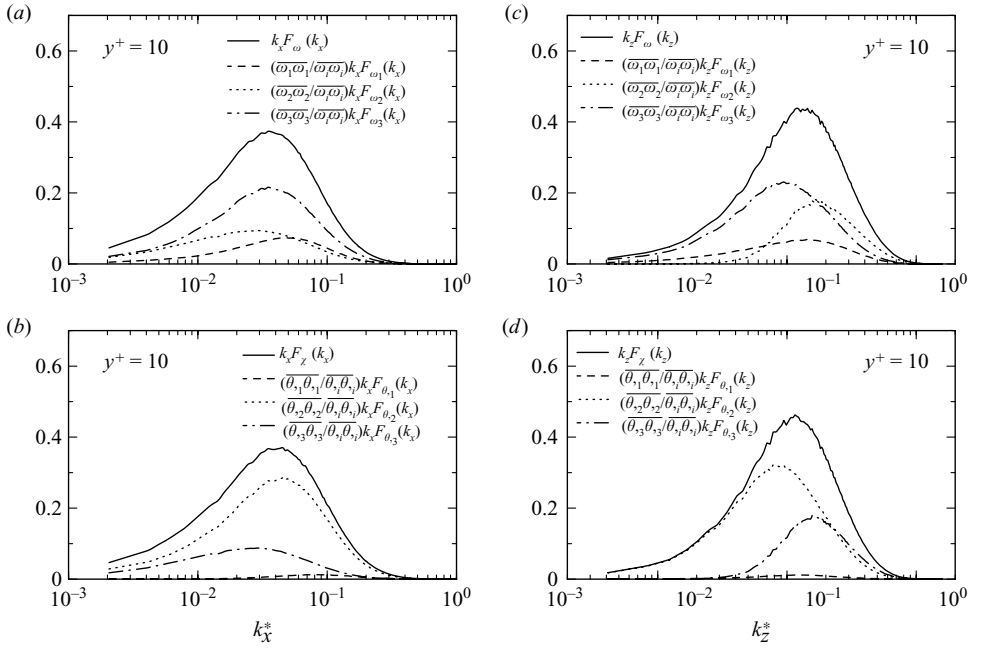

FIGURE 11. One-dimensional pre-multiplied spectral density of (*a*), (*c*) ω_i and (*b*), (*d*) $\theta_{,i}$ for $h^+ = 395$ at $y^+ = 10$: (*a*), (*b*) streamwise spectra; (*c*), (*d*) spanwise spectra.

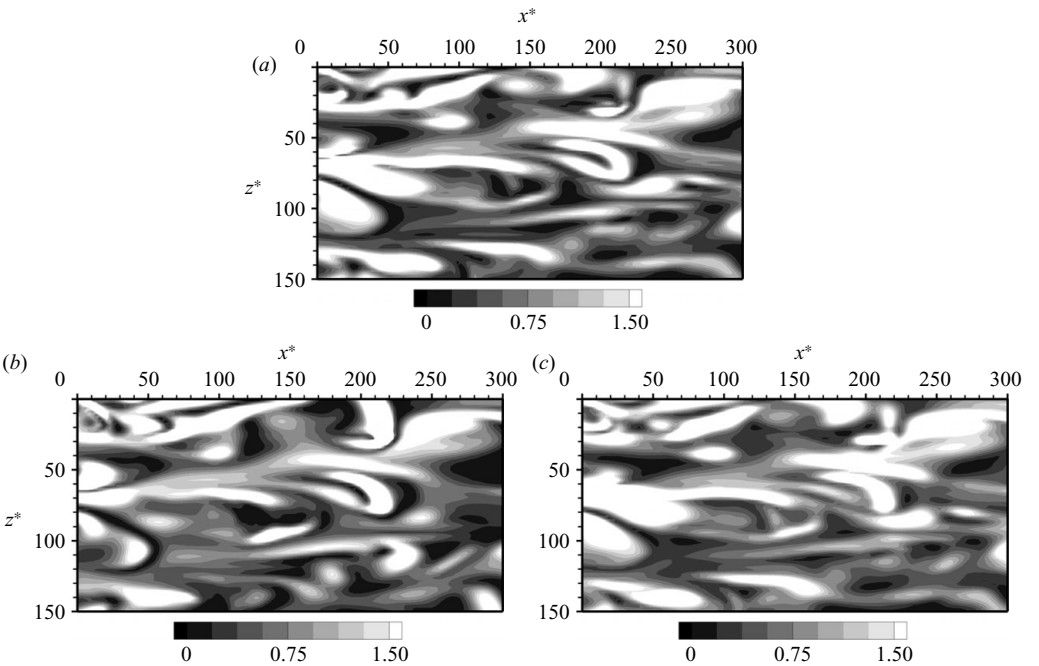

FIGURE 12. Instantaneous (x, z) isocontours of ω and χ for $h^+ = 640$ at $y^+ = 10$: (*a*) $\omega_i^2/\overline{\omega_i^2}$; (*b*) $\chi/\overline{\chi}$; (*c*) $\varepsilon/\overline{\varepsilon}$.

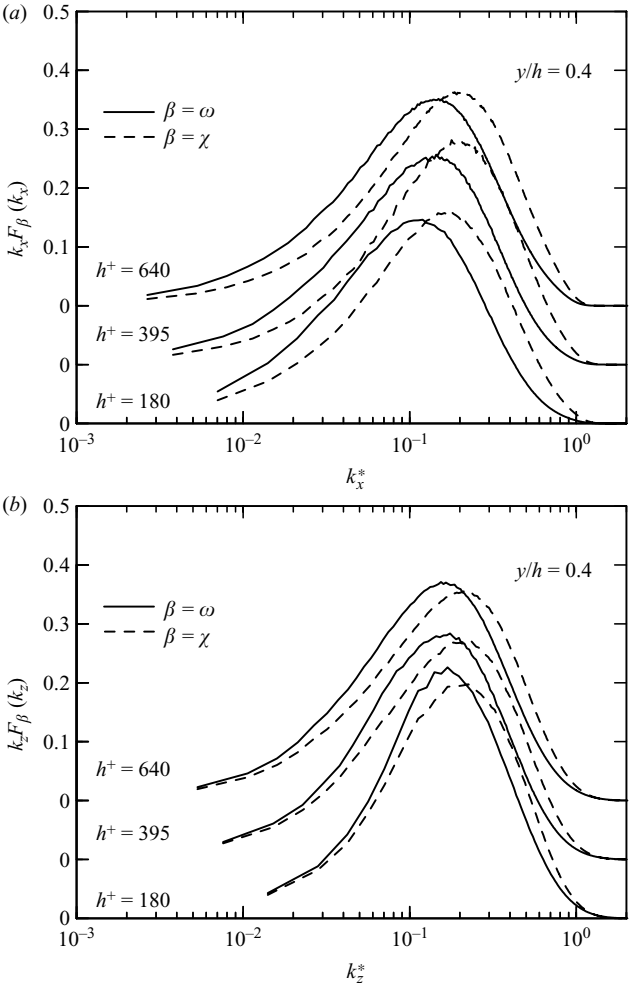

FIGURE 13. One-dimensional pre-multiplied spectral density of ω and χ for $h^+ = 180$, 395 and 640 at $y/h = 0.4$: (*a*) streamwise spectra; (*b*) spanwise spectra. Note the shift in origin for the ordinate. The lowest zero refers to $h^+ = 180$.

In the outer region, the similarity between F_ω and F_χ is inferior to that near the wall (see figures 10 and 13); the magnitude of F_χ at intermediate and high wavenumbers is slightly larger than that of F_ω (see figure 13), suggesting that the scalar dissipation rate is more intermittent than the enstrophy in this region. The impairment in the similarity between F_ω and F_χ in the outer region is worth discussing. Assuming local isotropy (e.g. Antonia & Kim 1994), each component of F_{ω_i} and $F_{\theta,i}$ is expected to contribute almost equally to F_ω and F_χ , respectively, as the centreline is approached. However, figure 14 reveals a clear difference between the relative contributions of F_{ω_i} to F_ω and those of $F_{\theta,i}$ to F_χ : the most energetic wavenumbers for two components of F_{ω_i} are nearly the same and larger than those for the remaining component, while the most energetic wavenumbers for two components of $F_{\theta,i}$ are almost equal and smaller than those for the remaining component. This difference may be associated with the anisotropy in the outer region: tubular structures in the vorticity field (Blackburn, Mansour & Cantwell 1996; Tanahashi *et al.* 2004) and sheet-like structures in the

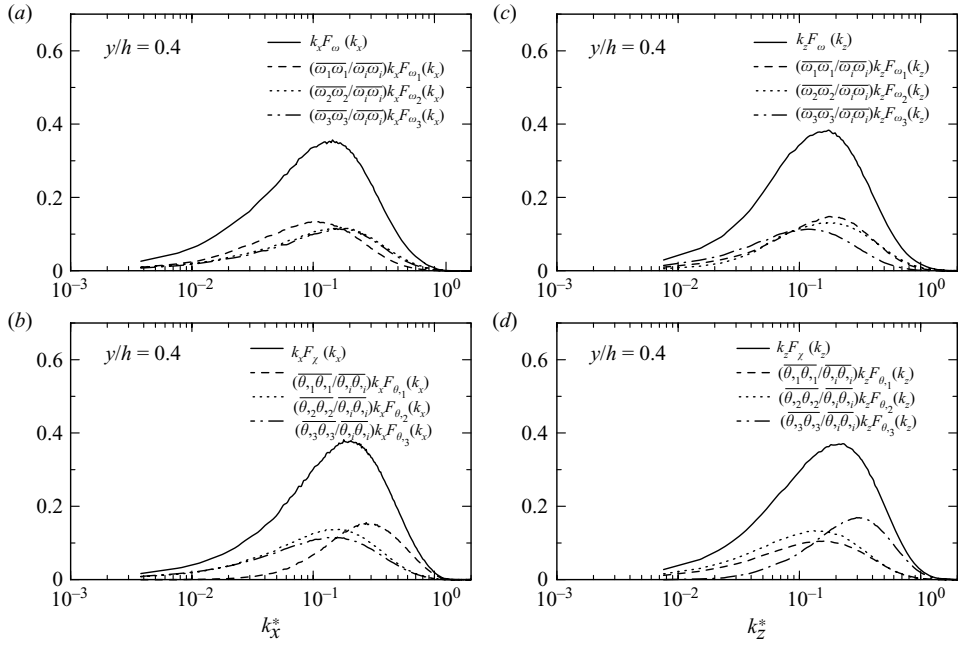

FIGURE 14. One-dimensional pre-multiplied spectral density of (*a*), (*c*) ω_i and (*b*), (*d*) $\theta_{,i}$ for $h^+ = 395$ at $y/h = 0.4$: (*a*), (*b*) streamwise spectra; (*c*), (*d*) spanwise spectra.

scalar dissipation rate field (Abe *et al.* 2006, 2009). Visualizations in the physical domain (figure 15) support this conjecture; the scalar dissipation rate exhibits more pronounced sheet-like structures than the enstrophy in this region. This is consistent with the finding that the vorticity and scalar gradient vectors align most preferentially with the directions of the intermediate and compressive principal rates of strain, respectively, in the outer region of this flow (Abe *et al.* 2008, 2009), the compressive strain generating the sheet-like structures in χ. Given that in the outer region ε is, to a large degree, only weakly correlated with ω_i^2 (see figure 15) and that the small-scale motion has many characteristics in common with other turbulent flows (Blackburn *et al.* 1996), one may wonder if ε exhibits sheet-like structures more clearly than ω_i^2. However, close inspection of the instantaneous realizations indicated that the sheet-like structures are more pronounced in χ than in either ω_i^2 or ε (see also Abe *et al.* 2009). The same trend was reported in homogeneous isotropic turbulence (e.g. Ashurst *et al.* 1987; Ruetsch & Maxey 1992; Pumir 1994; see also Sreenivasan & Antonia 1997). It seems reasonable to conclude that the impaired similarity between F_ω and F_χ in this region reflects the greater prominence of sheet-like structures for the scalar dissipation rate than the enstrophy.

Overall, the quality of the analogy between the enstrophy and the scalar dissipation rate is reasonable in both spectral and physical domains throughout the channel. This result supports the similarity between the transport equations of $\overline{\omega_i\omega_i}$ and $\overline{\theta_{,i}\,\theta_{,i}}$ when $Pr = 1$ (e.g. Corrsin 1953; Abe *et al.* 2008, 2009). Like the analogy between F_q and F_θ the analogy between F_ω and F_χ is marginally better in the near-wall region than in the outer region, suggesting that the presence of mean velocity and temperature gradients plays an important role in underpinning the spectral similarity between ω_i^2 and χ as well as that between $\boldsymbol{q}$ and θ.

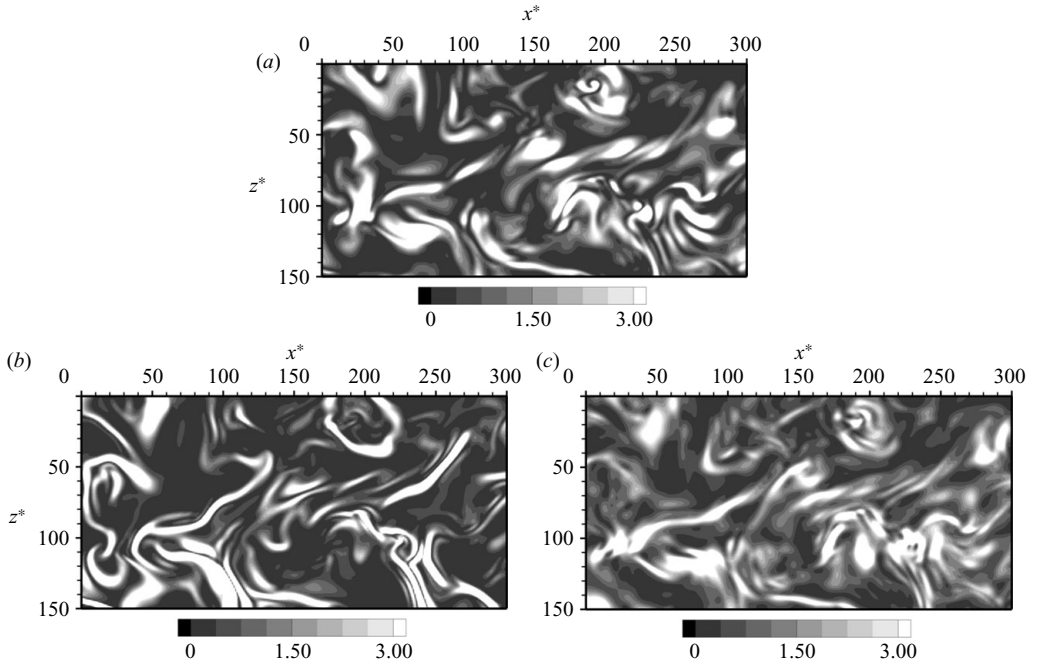

FIGURE 15. Instantaneous (x, z) isocontours of ω and χ for $h^+ = 640$ at $y/h = 0.4$: (a) $\omega_i^2/\overline{\omega_i^2}$; (b) $\chi/\overline{\chi}$; (c) $\varepsilon/\overline{\varepsilon}$.

5. Degree of similarity between F_q and F_θ and between F_ω and F_χ

In this section, we examine in more detail the level of similarity between the spectral densities corresponding to $\overline{q^2}$ and $\overline{\theta^2}$ and those which correspond to $\overline{\omega_i^2}$ and $\overline{\chi}$.

Figure 16 shows distributions of the ratio F_θ/F_q at several y locations across the channel, in terms of both $k_x h$ (figure 16*a*) and $k_z h$ (figure 16*b*). As might be inferred from figures 1 and 4, the magnitude of F_θ/F_q is very close to unity for $k_x h < 20$ (figure 16*a*), independent of y. For $k_z h < 20$, the scatter in F_θ/F_q (figure 16*b*) is slightly larger than that in figure 16(*a*) due to sharper spectral peaks in F_q than in F_θ (figure 4*b*). Since the major contribution to F_q (k_z) is from F_u (k_z) (figure 5*b*), the scatter in figure 16(*b*) reflects a slight difference between the spanwise organization of the large-scale u and θ structures, the width of the latter structures tending to be greater than that of the former, as discussed in § 3 (see figure 6). When $k_x h > 20$, the ratio increases, the rate of increase tending to be greater at larger values of y/h. This behaviour, which is also apparent in figure 16(*b*), suggests that for sufficiently small length scales, $\overline{\theta^2}$ is almost invariably more energetic than $\overline{q^2}$. This is consistent with the instantaneous visualizations of u and θ in figure 8 and underlines the unmixed nature of the scalar (§ 3).

The ratio F_χ/F_ω (figure 17) is roughly unity in the near-wall region for small and intermediate wavenumbers, in conformity with the reasonable similarity between F_ω and F_χ (figure 10). As the distance from the wall increases, the magnitude of F_χ/F_ω decreases at small wavenumbers and increases at large wavenumbers. The former trend suggests that ω_i^2 may be more clustered than χ in the outer region (see figure 15) and contains more energy at large scales than χ. On the other hand, the latter trend is related to the unmixedness of the scalar dissipation rate, which

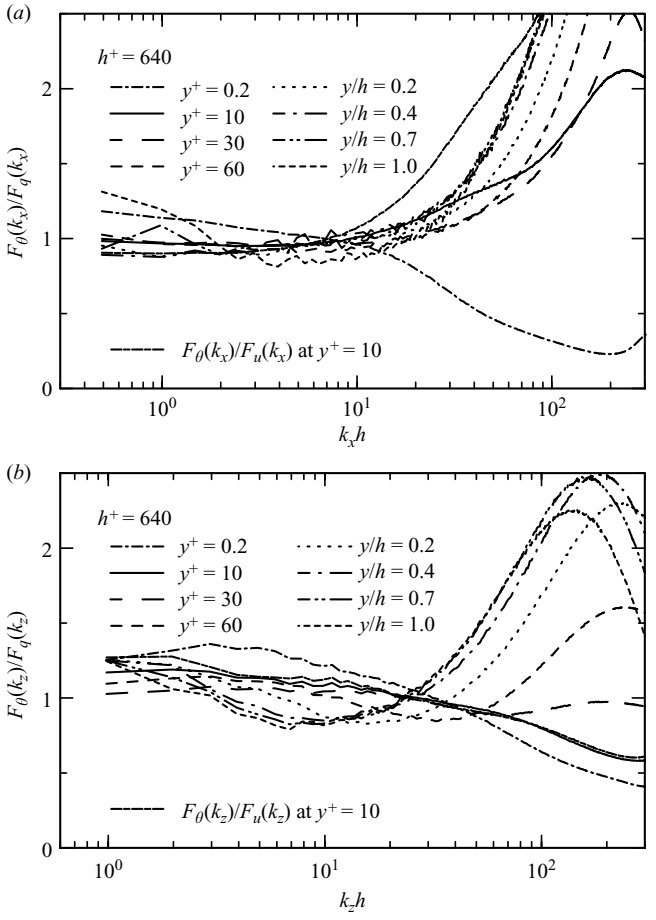

FIGURE 16. Distributions of the ratio of F_θ to F_q for $h^+ = 640$ at several y locations: (*a*) streamwise spectra; (*b*) spanwise spectra.

is associated with the sheet-like structures. The departure from unity of F_χ/F_ω is slightly smaller than that of F_θ/F_q (see figures 16 and 17).

In view of the reasonable similarity between F_q and F_θ, on one hand, and that between F_ω and F_χ, on the other, it is reasonable to assess the implications of these similarities on the distribution and magnitude of the time-scale ratio R,

$$R = \frac{\overline{\theta^2}}{\overline{q^2}}\frac{\overline{\varepsilon}}{\overline{\chi}}, \tag{5.1}$$

as well as the parameter B,

$$B = \frac{\overline{q^2}^{1/2}}{\overline{\theta^2}^{1/2}}\frac{\mathrm{d}\overline{\Theta}/\mathrm{d}y}{\mathrm{d}\overline{U}/\mathrm{d}y}. \tag{5.2}$$

The possibility that R remains constant, at least in a particular flow and at sufficiently large Reynolds numbers, would avoid the need to include a transport equation for the mean scalar dissipation rate. In his review, Launder (1976) suggested that the connection between the velocity and scalar time scales is 'not strong enough for the latter to serve generally as an approximation of the former', thus implying that a transport equation for $\overline{\chi}$ is also needed when modelling turbulent heat transport.

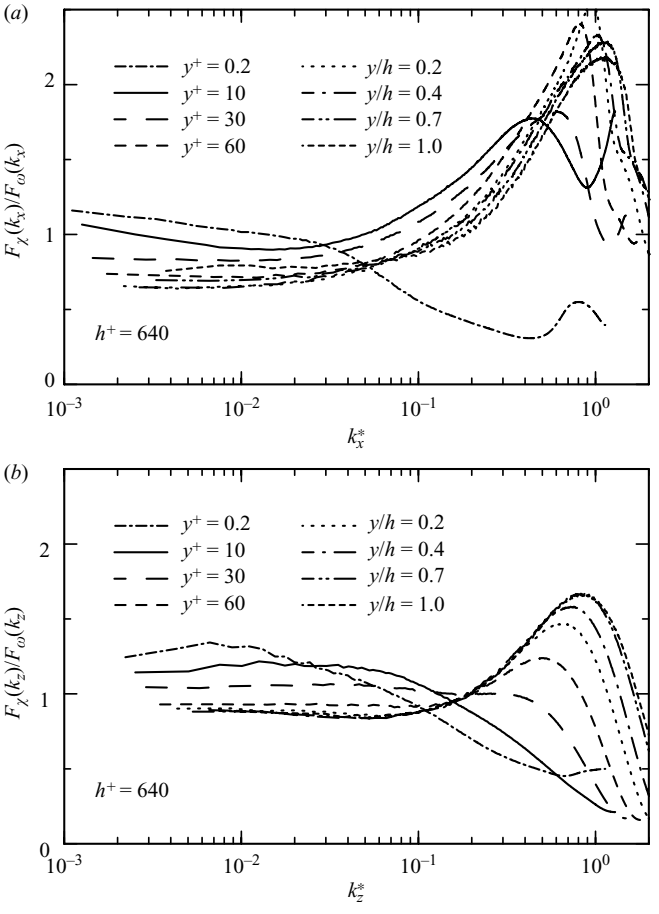

FIGURE 17. Distributions of the ratio of F_χ to F_ω for $h^+ = 640$ at several y locations: (*a*) streamwise spectra; (*b*) spanwise spectra.

The ratio R has been found to be reasonably constant, at least in near-equilibrium regions of turbulent shear flows (e.g. Béguier, Dekeyser & Launder 1978) and about 0.5–0.6 in the outer region of a turbulent channel flow at $Pr = 0.71$ (Kawamura *et al.* 2004). This constancy is also observed at other values of Pr, although the magnitude of R increases with increasing Pr (Kasagi & Ohtsubo 1993; Kawamura *et al.* 1998; Kawamura, Abe & Matsuo 1999; Kawamura *et al.* 2004). The near-wall limiting value of R can be obtained analytically and is equal to Pr (e.g. Kasagi *et al.* 1992; Kawamura *et al.* 1998, 1999). This value is also consistent with the similarity between $\overline{q^2}$ and $\overline{\theta^2}$ at the wall. By applying de l'Hopital's rule (noting that $\overline{\varepsilon}$ and $\overline{\chi}$ are non-zero at the wall)

$$\begin{aligned} \frac{\overline{\chi}_w}{\overline{\varepsilon}_w} R &= \lim_{y\to 0} \frac{\overline{\theta^2}}{\overline{q^2}} = \lim_{y\to 0} \frac{(\partial\overline{\theta^2}/\partial y)}{(\partial\overline{q^2}/\partial y)} \\ &= \frac{\overline{(\partial\theta/\partial y)^2}}{\overline{(\partial u/\partial y)^2} + \overline{(\partial w/\partial y)^2}} \\ &= Pr\,\frac{\overline{\chi}_w}{\overline{\varepsilon}_w}, \end{aligned} \tag{5.3}$$

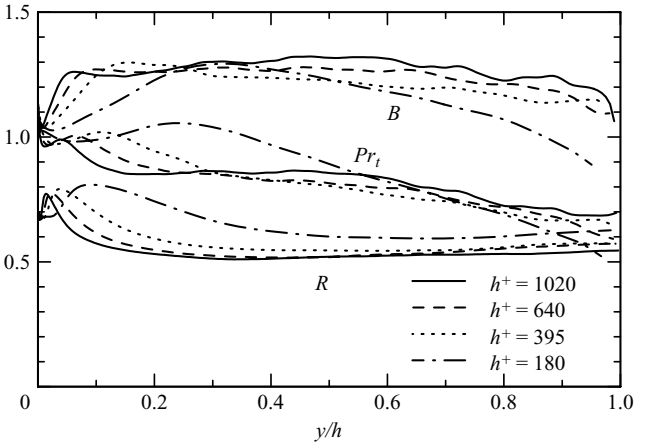

FIGURE 18. Distributions of the quantities R, B and Pr_t.

where the subscript w denotes a wall value. This result also implies $F_\theta/F_q = F_\chi/F_\omega$ at the wall. This can be inferred from figures 16 and 17, F_θ/F_q and F_χ/F_ω tending to follow each other closely as the wall is approached. The parameter B may be important in terms of estimating $\overline{\theta^2}$ in models which assume that the turbulent Prandtl number is constant. B has been found to be nearly constant (≈ 1.5) across most of the boundary layer (Fulachier & Dumas 1976). Figure 18 shows distributions of R and B across the channel. The turbulent Prandtl number Pr_t, defined by

$$\mathrm{Pr}_t = \frac{\overline{uv}}{\overline{v\theta}} \frac{\mathrm{d}\overline{\Theta}/\mathrm{d}y}{\mathrm{d}\overline{U}/\mathrm{d}y}, \tag{5.4}$$

is also included in the figure. Of the three quantities plotted, R exhibits the smallest variation throughout the channel and, except for $h^+ = 180$, is nearly independent of h^+. The parameter B is approximately constant (1.2–1.3) in the outer region, except near the centreline. For $h^+ = 1020$, R and B vary by about 5 % and 8 %, respectively, over the range $y/h = 0.2$–0.9. Replacing $\overline{u^2}^{1/2}$ by $\overline{q^2}^{1/2}$ in (5.2) reduces the difference between the inner and outer regions, but the percentage variation in the outer region is almost unchanged. However, the difference in magnitude between inner and outer regions is smaller for R than B; Pr_t displays the largest variation, tending to decrease slowly with increasing y/h. This variation can be satisfactorily described by a parabolic relation (not shown here), similar to that suggested by Rotta (1964). The DNS data of Bell & Ferziger (1993) in a turbulent boundary layer at small momentum thickness Reynolds numbers also show that Pr_t cannot be considered constant outside the near-wall region, the magnitude of Pr_t continuing to decrease in the outer region with increasing y/δ (δ is the boundary layer thickness). From a modelling viewpoint, figure 18 provides fairly strong support for setting R equal to a constant in the region $y/h > 0.2$, suggesting a linear relationship between the velocity ($k/\overline{\varepsilon}$) and temperature ($k_\theta/\overline{\chi}$) time scales, viz. $k_\theta/\overline{\chi} = c\,(k/\overline{\varepsilon})$ (where $k \equiv \overline{q^2}/2$, $k_\theta \equiv \overline{\theta^2}/2$ and c is a constant). By differentiating this relationship, the transport equation for $\overline{\chi}$ can be approximated by

$$\frac{\mathrm{D}\overline{\chi}}{\mathrm{D}t} = \frac{\overline{\chi}}{k_\theta}\frac{\mathrm{D}k_\theta}{\mathrm{D}t} + \frac{\overline{\chi}}{\overline{\varepsilon}}\frac{\mathrm{D}\overline{\varepsilon}}{\mathrm{D}t} - \frac{\overline{\chi}}{k}\frac{\mathrm{D}k}{\mathrm{D}t}. \tag{5.5}$$

A currently used model equation for $\overline{\chi}$ may be derived by substituting the model equations for k, ε and k_θ in (5.5) (see Johansson & Wikström 1999). The difference between R and Pr_t in the outer region may have implications when modelling the turbulent eddy diffusivity in the two-equation model for the scalar field (e.g. Nagano & Kim 1988; Yoshizawa 1988). In these models, Pr_t is obtained as

$$Pr_t = \frac{\nu_t}{a_t} = \frac{c_\mu}{c_\lambda} R^{-p}, \tag{5.6}$$

where

$$\nu_t = c_\mu \frac{k^2}{\varepsilon},\ a_t = c_\lambda \frac{k^2}{\varepsilon} R^p \tag{5.7}$$

(a_t and ν_t denote the turbulent eddy viscosity and diffusivity, respectively, and c_μ and c_λ represent model constants). Near-wall damping functions are omitted in (5.7), since the focus is on the outer region. Nagano & Kim (1988) used $p = 1/2$, whereas Yoshizawa (1988) used $p = 2$. The inclusion of R in the model implies using a mixture of velocity and scalar time scales. Unlike R, Pr_t varies in the outer region (figure 18); this means that (5.6) cannot be correct and needs to be revised. The two-equation heat transfer model of Nagano & Shimada (1996), which incorporates new velocity and time scales to represent various sizes of eddies in the velocity and thermal fields, shows promise, since the predicted Pr_t is in reasonable agreement with that obtained from the DNS data of Kim & Moin (1989).

In chapter 7 of Chassaing *et al.* (2002), (3.2) was rewritten as

$$\overline{q,_1^2} = \overline{u_{1,1}^2} + \overline{u_{2,1}^2} + \overline{u_{3,1}^2}. \tag{5.8}$$

It was argued that, using local isotropy, $\overline{\varepsilon}$ and $\overline{\chi}$ can be approximated by

$$\overline{\varepsilon}_{iso_q} = 3\nu\overline{q,_1^2}, \tag{5.9}$$

$$\overline{\chi}_{iso} = 3\kappa\overline{\theta,_1^2}. \tag{5.10}$$

With the use of (5.9) and (5.10), (5.1) may be rewritten as

$$R_{iso_q} = Pr \frac{\overline{\theta^2}}{\overline{q^2}} \frac{\overline{q,_1^2}}{\overline{\theta,_1^2}}, \tag{5.11}$$

and hence

$$R_{iso_q} = Pr \frac{\int_0^\infty k_x^2 F_q(k_x)\,\mathrm{d}k_x}{\int_0^\infty k_x^2 F_\theta(k_x)\,\mathrm{d}k_x}. \tag{5.12}$$

If the spectral analogy were perfect, viz. $F_q(k_x) = F_\theta(k_x)$ (or presumably $F_q(k_z) = F_\theta(k_z)$), then $R_{iso_q} = Pr$. Local isotropy is a reasonable approximation over a significant portion of the outer layer. However, in this region $F_q(k_x)$ is smaller than $F_\theta(k_x)$ especially at sufficiently large values of k_x (figure 16). As a consequence, the inequality

$$R_{iso_q} < Pr \tag{5.13}$$

holds in the outer region and is consistent with the magnitude of the time-scale ratio in this region (figure 18).

It is difficult to estimate R accurately from experimental data, since estimates of $\overline{\varepsilon}$ and $\overline{\chi}$ are almost invariably incomplete and often unreliable. In this context, it seems appropriate to test the assumptions of local isotropy as well as local axisymmetry (Batchelor 1946; Chandrasekhar 1950; George & Hussein 1991), since they have been

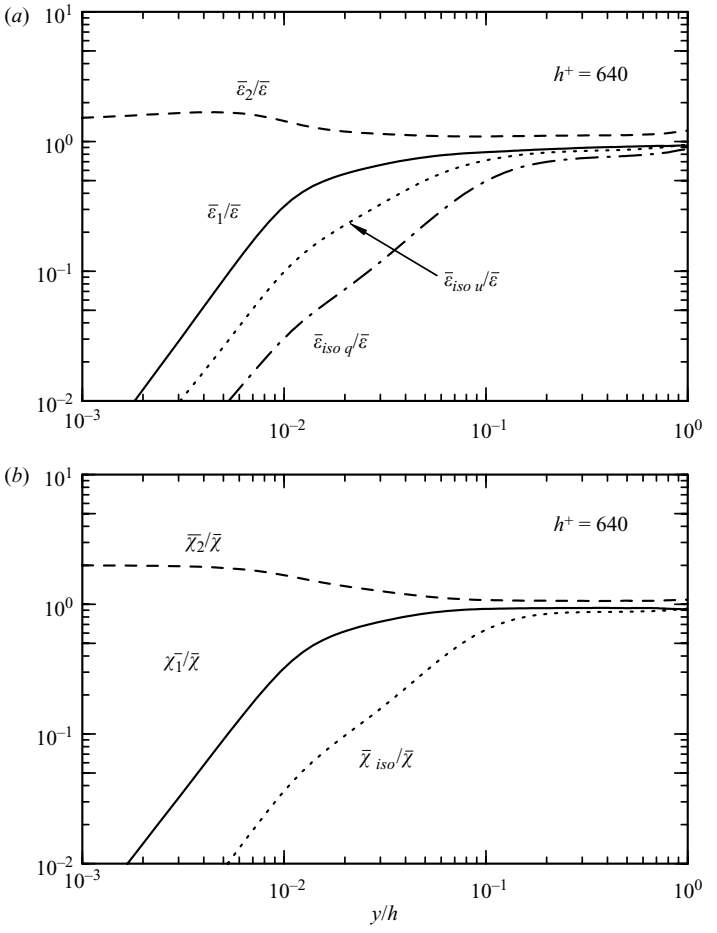

FIGURE 19. Distributions of the ratios $\overline{\varepsilon}_{iso}/\overline{\varepsilon}$, $\overline{\chi_{iso}}/\overline{\chi}$, $\overline{\varepsilon}_1/\overline{\varepsilon}$, $\overline{\varepsilon}_2/\overline{\varepsilon}$, $\overline{\chi}_1/\overline{\chi}$, $\overline{\chi}_2/\overline{\chi}$.

used to simplify $\overline{\varepsilon}$ and $\overline{\chi}$. Their locally isotropic forms are given by (5.9) and (5.10) as well as the well-known expression

$$\overline{\varepsilon}_{iso_u} = 15\nu\overline{u_{1,1}^2}. \tag{5.14}$$

The locally axisymmetric relations (with x_1 as the preferred axis) are

$$\overline{\varepsilon}_1 = \nu\left(\frac{5}{3}\overline{u_{1,1}^2} + 2\overline{u_{1,3}^2} + 2\overline{u_{2,1}^2} + \frac{8}{3}\overline{u_{2,3}^2}\right), \tag{5.15}$$

$$\overline{\varepsilon}_2 = \nu\left(-\overline{u_{1,1}^2} + 2\overline{u_{1,2}^2} + 2\overline{u_{2,1}^2} + 8\overline{u_{2,2}^2}\right), \tag{5.16}$$

$$\overline{\chi}_1 = \kappa\left(\overline{\theta,_1^2} + 2\overline{\theta,_3^2}\right), \tag{5.17}$$

$$\overline{\chi}_2 = \kappa\left(\overline{\theta,_1^2} + 2\overline{\theta,_2^2}\right). \tag{5.18}$$

Expressions (5.15) and (5.16) were first written by George & Hussein (1991). Comparative checks of local isotropy and local axisymmetry are provided in figure 19 through the distributions of $\overline{\varepsilon}_{iso_q}/\overline{\varepsilon}$, $\overline{\varepsilon}_{iso_u}/\overline{\varepsilon}$, $\overline{\chi}_{iso}/\overline{\chi}$, $\overline{\varepsilon}_1/\overline{\varepsilon}$, $\overline{\varepsilon}_2/\overline{\varepsilon}$, $\overline{\chi}_1/\overline{\chi}$, $\overline{\chi}_2/\overline{\chi}$. The locally axisymmetric expressions of $\overline{\varepsilon}_2/\overline{\varepsilon}$ and $\overline{\chi}_2/\overline{\chi}$ are close to unity throughout the channel,

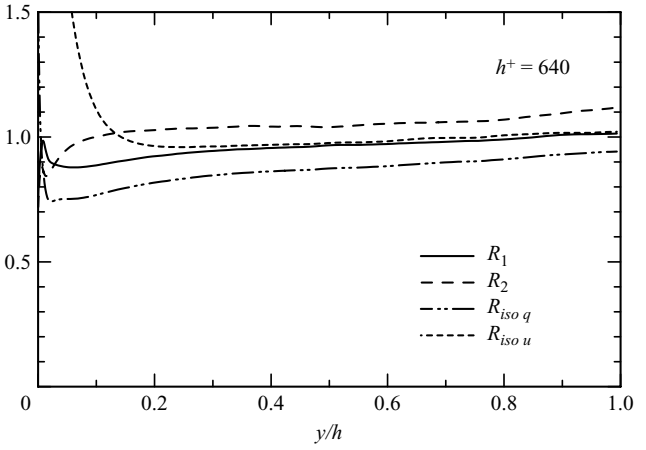

FIGURE 20. Distributions of R, as obtained from relations (5.11), (5.19) and (5.20). In each case, R is divided by its 'correct' value, given by the relation (5.1).

consistent with the finding by Antonia *et al.* (1991) that local axisymmetry is more appropriate than local isotropy in the near-wall region of this flow. However, $\overline{\varepsilon}_{iso_u}/\overline{\varepsilon}$ and $\overline{\chi}_{iso}/\overline{\chi}$ are nearly unity for $y/h > 0.2$, in support of local isotropy in this region of the flow. The departure from unity of $\overline{\varepsilon}_{iso_q}/\overline{\varepsilon}$ is larger than that of $\overline{\varepsilon}_{iso_u}/\overline{\varepsilon}$ except near the centreline, suggesting that, within the framework of local isotropy, $\overline{\varepsilon}_{iso_u}$ is more adequate than $\overline{\varepsilon}_{iso_q}$.

We now turn our attention to assessing the locally isotropic and axisymmetric forms for R. The locally isotropic form of R is given by (5.11) as well as by

$$R_{iso_u} = Pr\frac{\overline{\theta^2}}{\overline{q^2}}\frac{5\overline{u_{1,1}^2}}{\overline{\theta_{,1}^2}}. \tag{5.19}$$

The locally axisymmetric expressions for R are

$$R_1 = \frac{\overline{\theta^2}}{\overline{q^2}}\frac{\overline{\varepsilon}_1}{\overline{\chi}_1},\ R_2 = \frac{\overline{\theta^2}}{\overline{q^2}}\frac{\overline{\varepsilon}_2}{\overline{\chi}_2}. \tag{5.20}$$

Distributions of the isotropic ((5.11) and (5.19) and axisymmetric (5.20) forms of R divided by R (5.1) are given in figure 20. As inferred from figure 19, the assumption of local axisymmetry (5.20) is superior to assuming local isotropy and should therefore provide a more reliable means of estimating R than (5.19) almost throughout the channel. Local isotropy remains a reasonable approximation in the outer region ($y/h > 0.2$), thus allowing experimenters to use (5.19), which is more easily determined experimentally than (5.20), in this part of the flow.

6. Conclusions

The relationship between the fluctuating velocity vector, $\boldsymbol{q}$, and the temperature fluctuation, θ, has been examined using DNS databases of a turbulent channel flow with a passive scalar for a constant heat-flux boundary condition (Abe *et al.* 2004*b*, 2008, 2009) at $Pr = 0.71$ and four values of h^+(180, 395, 640 and 1020). The possibility of a spectral analogy between scales associated with the dissipation rates for the velocity and scalar fields has also been explored. The following conclusions can be drawn:

(i) The spectral analogy between $\boldsymbol{q}$ and θ is reasonable throughout the channel, consistent with the earlier boundary layer results of Fulachier & Dumas (1976). Except perhaps at the two lower Reynolds numbers, this similarity is not affected significantly by h^+ except for the spanwise spectral analogy at $h^+ = 180$ and 395. In the inner region, it is u which is the dominant contributor to the $\boldsymbol{q}$ spectrum irrespective of whether the spectra are viewed in terms of k_x or k_z. In the outer region, the streamwise similarity between $\boldsymbol{q}$ and θ reflects the sum of the similarities between u and θ, v and θ and also w and θ, while the spanwise spectral similarity between $\boldsymbol{q}$ and θ reflects mainly the similarity between u and θ.

(ii) The instantaneous isocontours of q^2 and θ^2 in the (x, y), (x, z) and (y, z) planes are consistent with the spectral similarity, although, in the outer region, the similarity in physical space is, arguably, not as good as the spectral similarity. In the latter region, the similarity between q^2 and θ^2 in physical space is prominent mainly for large magnitudes of these two quantities. Further, differences between the large-scale structures of u and θ are observed in the outer region (figures 6 and 8). The spanwise extent of the large-scale θ structures is bigger than that of the large-scale u structures. The inclination of the large-scale θ structures to the wall is much steeper than that of the large-scale u structures. The interface between positive and negative values of θ is sharper than that between positive and negative values of u, emphasizing the unmixed nature of the scalar.

(iii) The analogy between F_ω and F_χ is good in the inner region although of slightly poorer quality than that between the spectra of ω_2 and $\theta_{,3}$ or between those of ω_3 and $\theta_{,2}$. The good agreement for the latter two cases is closely related to the almost excellent spatial coincidence between velocity and thermal streaks (Abe *et al.* 2006, 2009). When plotted against k_z, the comparison between F_ω and F_χ is generally poorer than that between F_q and F_θ. When plotted against k_x, the agreement between F_ω and F_χ is at least as good, if not better, than that between F_q and F_θ. Overall, the spectral analogy, either between F_q and F_θ or between F_ω and F_χ , tends to deteriorate as the centreline of the channel is approached when the magnitude of the wavenumber (either k_x or k_z) increases. This trend is most likely associated with the reduced level of forcing of the velocity and temperature fields, i.e. the reduction in the magnitudes of the mean velocity and temperature gradients in this region. For scales comparable to the Kolmogorov length scale, the magnitude of F_θ is larger than that of F_q. Similarly, the magnitude of F_χ is larger than that of F_ω. This implies that the lack of mixedness of the scalar is manifested by the existence of the scalar sheets and ensures that the spectral similarity breaks down at large wavenumbers.

(iv) As a result of the reasonable similarity, almost right across the channel, between F_q and F_θ on one hand and between F_ω and F_χ on the other, R varies much less with respect to y than either the parameter B or the turbulent Prandtl number, Pr_t. The latter tends to decrease slowly with increasing y/h, whereas R is approximately constant for $y/h > 0.1$ and is less affected by low-Reynolds-number effects than Pr_t. From a modelling viewpoint, the assumption $Pr_t =$ constant would not be as accurate as assuming that R is constant. The constancy of R appears robust, since it is underpinned by the similarity – well documented in this paper – in both physical space and the spectral domain. It should be noted however that this constancy may not apply when Pr is much larger or much smaller than 1, since it is unlikely that the analogy will apply for large and small values of the molecular Prandtl number. The ratio R has been shown to equal Pr at the wall. The similarity between $\overline{q^2}$ and $\overline{\theta^2}$ (see (5.3)) is consistent with this result. Using (5.12) and the ratios F_θ/F_q and F_χ/F_ω the magnitude of R has been shown to satisfy the inequality $R < Pr$ in the outer region

of this flow. This inequality most likely reflects the unmixedness of the scalar. The assumptions of local isotropy and local axisymmetry have been tested in the context of estimating R experimentally. Overall, there is little doubt that local axisymmetry is superior to local isotropy over a significant portion of the channel. Nonetheless, local isotropy (5.19) is a reasonable approximation in the outer region and should therefore continue to provide a useful and simple way of estimating R from only measurements of streamwise derivatives of velocity and scalar fluctuations in this region.

Computations performed on Numerical Simulator III at the Computer Centre of the Japan Aerospace Exploration Agency are gratefully acknowledged. HA was partially supported by the Ministry of Education, Science, Sports and Culture Grant-in-Aid for Young Scientists (B) 20760125 (2008). RAA acknowledges the support of the Australian Research Council.

REFERENCES

Abe, H., Antonia, R. A. & Kawamura, H. 2006 Structure of the scalar dissipation field in a turbulent channel flow. In *Proc. of Turbulence, Heat and Mass Transfer Conf. 5*, Dubrovnik, Croatia.

Abe, H., Antonia, R. A. & Kawamura, H. 2008 Transport equations for the enstrophy and scalar dissipation rate in a turbulent channel flow. In *Proc. of 7th Intl ERCOFTAC Symp. on Engng Turbulence Modelling and Measurements*, Limassol, Cyprus.

Abe, H., Antonia, R. A. & Kawamura, H. 2009 Correlation between small-scale velocity and scalar fluctuations in a turbulent channel flow. *J. Fluid Mech.* **627**, 1–32.

Abe, H., Kawamura, H. & Choi, H. 2004*a* Very large-scale structures and their effects on the wall shear-stress fluctuations in a turbulent channel flow up to $Re_\tau = 640$. *ASME J. Fluids Engng* **126**, 835–843.

Abe, H., Kawamura, H. & Matsuo, Y. 2001 Direct numerical simulation of a fully developed turbulent channel flow with respect to the Reynolds number dependence. *ASME J. Fluids Engng* **123**, 382–393.

Abe, H., Kawamura, H. & Matsuo, Y. 2004*b* Surface heat-flux fluctuations in a turbulent channel flow up to $Re_\tau = 1020$ with $Pr = 0.025$ and 0.71. *Intl J. Heat and Fluid Flow* **25**, 404–419.

del Álamo, J. C. & Jiménez, J. 2003 Spectra of the very large anisotropic scales in turbulent channels. *Phys. Fluids* **15**, 41–44.

del Álamo, J. C., Jiménez, J., Zandonade, P. & Moser, R. D. 2004 Scaling of the energy spectra of turbulent channels. *J. Fluid Mech.* **500**, 135–144.

Antonia, R. A, Chambers, A. J., Friehe, C. A & Van Atta, C. W. 1979 Temperature ramps in the atmospheric surface layer. *J. Atmos. Sci.* **36**, 99–108.

Antonia, R. A. & Kim, J. 1991 Similarity between turbulent kinetic energy and temperature spectra in the near-wall region. *Phys. Fluids* **276**, 989–991.

Antonia, R. A., Kim, J. & Browne, L. W. B. 1991 Some characteristics of small-scale turbulence in a turbulent duct flow. *J. Fluid Mech.* **233**, 369–388.

Antonia, R. A. & Kim, J. 1994 A numerical study of local isotropy of turbulence. *Phys. Fluids* **6** (2), 834–841.

Antonia, R. A., Krishnamoorthy, L. V. & Fulachier, L. 1988 Correlation between the longitudinal velocity fluctuation and temperature fluctuation in the near-wall region of a turbulent boundary layer. *Intl J. Heat Mass Transfer* **31** (4), 723–730.

Antonia, R. A., Rajagopalan, S., Subramanian, C. S. & Chambers, A. J. 1982 Reynolds-number dependence of the structure of a turbulent boundary layer. *J. Fluid Mech.* **121**, 123–140.

Antonia, R. A., Ould-Rouis, M., Anselmet, F. & Zhu, Y. 1997 Analogy between predictions of Kolmogorov and Yaglom. *J. Fluid Mech.* **332**, 395–409.

Antonia, R. A., Zhou, T. & Zhu, Y. 1998 Three-component vorticity measurements in a turbulent grid flow. *J. Fluid Mech.* **374**, 29–57.

Antonia, R. A., Zhu, Y., Anselmet, F. & Ould-Rouis, M. 1996 Comparison between the sum of the second-order velocity structure functions and the second-order temperature structure function. *Phys. Fluids* **8**, 3105–3111.

Ashurst, W. T., Kerstein, A. R., Kerr, R. M. & Gibson, C. H. 1987 Alignment of vorticity and scalar gradient with strain rate in simulated Navier–Stokes turbulence. *Phys. Fluids* **30**, 2343–2353.

Batchelor, G. K. 1946 The theory of axisymmetric turbulence. *Proc. R. Soc. Lond.* A **186**, 480–502.

Batchelor, G. K. 1959 Small-scale variation of convected quantities like temperature in turbulent fluid. Part 1. General discussion and the case of small conductivity. *J. Fluid Mech.* **5**, 113–133.

Béguier, C., Dekeyser, I. & Launder, B. E. 1978 Ratio of scalar and velocity dissipation time scales in shear flow turbulence. *Phys. Fluids* **21**, 307–310.

Bell, D. M. & Ferziger, J. H. 1993 Turbulent Boundary Layer DNS with passive scalars. In *Near-Wall Turbulent Flows* (ed. R. M. C. So, C. G. Speziale & B. E. Launder), pp. 327–336. Elsevier Science.

Blackburn, H. M., Mansour, N. N. & Cantwell, B. J. 1996 Topology of fine-scale motions in turbulent channel flow. *J. Fluid Mech.* **310**, 269–292.

Brown, G. L. & Thomas, A. S. W. 1977 Large structure in a turbulent boundary layer. *Phys. Fluids* **20** (10), S243–S252.

Burattini, P. & Antonia, R. A. 2005 Approach to the 4/5 and 4/3 laws for nearly homogeneous and isotropic turbulence. In *Eighth Australasian Heat and Mass Transfer Conf.*, Curtin University of Technology, Perth, Western Australia.

Chandrasekhar, S. 1950 The theory of axisymmetric turbulence. *Proc. R. Soc. Lond.* A **242**, 557–577.

Chassaing, P., Antonia, R. A., Anselmet, F., Joly, L. & Sarkar, S. 2002 *Variable Density Fluid Turbulence*, Kluwer Academic.

Chen, C.-H. P. & Blackwelder, R. F. 1978 Large-scale motion in a turbulent boundary layer: a study using temperature contamination. *J. Fluid Mech.* **89**, 1–31.

Christensen, K. T. & Adrian, R. J. 2001 Statistical evidence of hairpin vortex packets in wall turbulence. *J. Fluid Mech.* **431**, 433–443.

Corrsin, S. 1951 On the Spectrum of isotropic temperature fluctuations in an isotropic turbulence. *J. Appl. Phys.* **22**, 469–473.

Corrsin, S. 1953 Remarks on turbulent heat transfer: an account of some features of the phenomenon in fully turbulent regions. In *Proc. of the First Iowa Thermodynamics Symp.*, pp. 5–30. State University of Iowa, Iowa City.

Fulachier, L. & Antonia, R. A. 1984 Spectral analogy between temperature and velocity fluctuations in several turbulent flows. *Intl J. Heat Mass Transfer* **27**, 987–997.

Fulachier, L. & Dumas, R. 1976 Spectral analogy between temperature and velocity fluctuations in a turbulent boundary layer. *J. Fluid Mech.* **77**, 257–277.

George, W. K. & Hussein, H. J. 1991 Locally axisymmetric turbulence. *J. Fluid Mech.* **233**, 1–23.

Guezennec, Y., Stretch, D. & Kim, J. 1990 The structure of turbulent channel flow with passive scalar transport. In *Proc. of the Summer Program 1990*, Centre for Turbulence Research, pp. 127–138. Stanford University.

Hoyas, S. & Jiménez, J. 2008 Reynolds number effects on the Reynolds-stress budgets in turbulent channels. *Phys. Fluids* **20**, 101511.

Hutchins, N. & Marusic, I. 2007 Evidence of very long meandering features in the logarithmic region of turbulent boundary layers. *J. Fluid Mech.* **579**, 1–28.

Iritani, Y., Kasagi, N. & Hirata, M. 1985 Heat transfer mechanism and associated turbulence structure in the near-wall region of a turbulent boundary layer. In *Turbulent Shear Flows 4* (ed. L. J. S. Bradbury, F. Durst, B. E. Launder, F. W. Schmidt and J. H. Whitelaw), pp. 223–234. Springer.

Jiménez, J. 1998 The largest scales of turbulent wall flows. In *CTR Annual Research Briefs*, pp. 137–154. Stanford University.

Johansson, A. V. & Wikström, P. M. 1999 DNS and modelling of passive scalar transport in turbulent channel flow with a focus on scalar dissipation rate modelling. *Flow Turbulence Combust.* **63**, 223–245.

Kader, B. A. 1981 Temperature and concentration profiles in fully turbulent boundary layers. *Intl J. Heat Mass Transfer* **24**, 1541–1544.

Kasagi, N. & Ohtsubo, Y. 1993 Direct numerical simulation of low Prandtl number thermal field in a turbulent channel flow. In *Turbulent Shear Flows 8* (ed. F. Durst, R. Friedrich, B. E. Launder, F. W. Schmidt, U. Schumann and J. H. Whitelaw), pp. 97–119. Springer.

Kasagi, N. Tomita, Y. & Kuroda, A. 1992 Direct numerical simulation of passive scalar field in a turbulent channel flow. *ASME J. Heat Transfer* **144**, 598–606.

Kawamura, H., Abe, H. & Matsuo, Y. 1999 DNS of turbulent heat transfer in channel flow with respect to Reynolds and Prandtl number effects. *Intl J. Heat Fluid Flow* **20**, 196–207.

Kawamura, H., Abe, H. Matsuo, Y. & Choi, H. 2002 Large-scale structures of velocity and scalar fields in turbulent channel flows. In *Intl Symp. on Dynamics and Statistics of Coherent Structures in Turbulence: Roles of Elementary Vortices* pp. 49–64, Tokyo.

Kawamura, H., Abe, H. & Matsuo, Y. 2004 Very large-scale structures observed in DNS of turbulent channel flow with passive scalar transport. In *Proc. of 15th Australasian Fluid Mech. Conf.*, The University of Sydney, Sydney, Australia.

Kawamura, H., Ohsaka, K., Abe, H. & Yamamoto, K. 1998 DNS of turbulent heat transfer in channel flow with low to medium–high Prandtl number fluid. *Intl J. Heat Fluid Flow* **19**, 482–491.

Kim, J. & Moin. P. 1989 Transport of passive scalars in a turbulent channel flow. In *Turbulent Shear Flows 6*, (ed. J.-C. André, J. Cousteix, F. Durst, B. E. Launder, F. W. Schmidt and J. H. Whitelaw), pp. 85–96, Springer.

Krogstad, P.-Å. & Antonia, R. A. 1994 Structure of turbulent boundary layers on smooth and rough walls. *J. Fluid Mech.* **277**, 1–21.

Launder, B. E. 1976 Heat and mass transport *Topics Appl. Phys.* **12**, 231–287.

Moin, P. & Mahesh, K. 1998 Direct numerical simulation: a tool in turbulence research. *Annu. Rev. Fluid Mech.* **30**, 539-578.

Morinishi, Y., Lund, T. S., Vasilyev, O. V. & Moin, P. 1998 Fully conservative higher order finite difference schemes for incompressible flow. *J. Comput. Phys.* **143**, 90–124.

Nagano, Y. & Kim, C. 1988 A two-equation model for heat transport in wall turbulent shear flows. *ASME J. Heat Transfer* **110**, 583–589.

Nagano, Y. & Shimada, M. 1996 Development of a two-equation heat transfer model based on direct simulations of turbulent flows with different Prandtl numbers. *Phys. Fluids* **8**, 3379–3402.

Pumir, A. 1994 A numerical study of the mixing of a passive scalar in three dimensions in the presence of a mean gradient. *Phys. Fluids* **6** (6), 2118–2132.

Rajagopalan, S. & Antonia, R. A. 1979 Some properties of the large structure in a fully developed turbulent duct flow. *Phys. Fluids* **22** (4), 614–622.

Robinson, S. K. 1991 The kinematics of turbulent boundary layer structure. *Tech Rep.* TM103859. NASA.

Rotta, J. C. 1964 Temperaturverteilungen in der turbulenten grenzschicht an der ebenen platte. *Intl J. Heat Mass Transfer* **7**, 215–228.

Ruetsch, G. R. & Maxey, M. R. 1992 The evolution of small-scale structures in homogeneous isotropic turbulence. *Phys. Fluids* A **4**, 2747–2760.

Spalart, P. R., Moser, R. D. & Rogers, M. M. 1991 Spectral methods for the Navier–Stokes equations with one infinite and two periodic directions. *J. Comput. Phys.* **96**, 297–324.

Sreenivasan, K. R. & Antonia, R. A. 1997 The phenomenology of small-scale turbulence. *Annu. Rev. Fluid Mech.* **29**, 435–472.

Subramanian, C. S., Rajagopalan, S., Antonia, R. A. & Chambers, A. J. 1982 Comparison of conditional sampling and averaging techniques in a turbulent boundary layer. *J. Fluid Mech.* **123**, 335–362.

Tanahashi, M., Kang, S.-J., Miyamoto, T., Shiokawa, S. & Miyauchi, T. 2004 Scaling law of fine scale eddies in turbulent channel flows up to $Re_\tau = 800$. *Intl J. Heat Fluid Flow* **25**, 331–340.

Tavoularis, S. & Corrsin, S. 1981 Experiments in nearly homogeneous shear flow with a uniform mean temperature gradient. Part 1. The fine structure. *J. Fluid Mech.* **104**, 311–347.

Taylor, R. J. 1958 Thermal structures in the lowest layers of the atmosphere. *Aust. J. Phys.* **11**, 168–176.

Warhaft, Z. 2000 Passive scalars in turbulent flows. *Annu. Rev. Fluid Mech.* **32**, 203–240.

Yoshizawa, A. 1988 Statistical modelling of passive-scalar diffusion in turbulent shear flows. *J. Fluid Mech.* **195**, 541–555.